Canonical and non-canonical contributions of human Dicer helicase domain in antiviral defense

Morgane Baldaccini, Léa Gaucherand, Béatrice Chane-Woon-Ming, Mélanie Messmer, Floriane Gucciardi, Sébastien Pfeffer*

Université de Strasbourg, Architecture et Réactivité de l'ARN, Institut de Biologie Moléculaire et Cellulaire du CNRS, 67000 Strasbourg, France

* To whom correspondence should be addressed: s.pfeffer@ibmc-cnrs.unistra.fr

ABSTRACT

In mammals, the co-existence of RNAi and the type I interferon response in somatic cells begs the question of their compatibility and relative contribution during viral infection. Previous studies provided hints that both mitigating co-factors and self-limiting properties of key proteins such as Dicer could explain the apparent inefficiency of antiviral RNAi. Indeed, the helicase domain of human Dicer limits its processing activity and acts as an interaction platform for co-factors that could hinder its function. We studied the involvement of several helicase-truncated mutants of human Dicer in the antiviral response. We show that all deletion mutants display an antiviral phenotype against alphaviruses and an enterovirus. While only one of them, Dicer N1, is antiviral in an RNAi-independent manner, they all require the expression of PKR to be active. To elucidate the mechanism underlying the antiviral phenotype of Dicer N1 expressing cells, we analyzed their transcriptome and found that many genes from the interferon and inflammatory response were upregulated. We could show that these genes appear to be controlled by transcription factors such as STAT-1, STAT-2, and NF-kB. Finally, we demonstrated that blocking the NF-kB pathway in Dicer N1 cells abrogated their antiviral phenotype. Our findings highlight the crosstalk between Dicer, PKR, and the IFN-I pathway, and suggest that human Dicer may have repurposed its helicase domain to prevent basal activation of antiviral and inflammatory pathways.

32 **INTRODUCTION**

33 RNAi is an evolutionary conserved cellular defense mechanism against invading nucleic acids.
34 It is based on the detection and cleavage of a trigger molecule, double-stranded (ds) RNA, by
35 Dicer, a type III ribonuclease. The resulting small interfering (si) RNAs act as guides for
36 effector Argonaute proteins that will act on target RNAs in a sequence specific manner (Meister
37 & Tuschl, 2004). By its nature, RNAi has been shown to be a prominent defense mechanism
38 against viruses in plant and invertebrate organisms (Guo *et al*, 2019; tenOever, 2016), but its
39 exact contribution to the innate antiviral response in mammals remains to be firmly established.
40 Although antiviral RNAi appears to be active in specific conditions, in particular in pluripotent
41 stem cells (Maillard *et al*, 2013), it also seems to be incompatible with other innate immune
42 defense pathways that rely on the type I interferon response (IFN-I). As a result, certain studies
43 have shown that inactivating then IFN-I response allows RNAi to take over. The pattern
44 recognition receptors that are inactivated in these studies are members of the RIG-I like
45 receptors (RLR) family and they are also activated by dsRNA (Ahmad & Hur, 2015; Pichlmair
46 & Reis e Sousa, 2007). However, as opposed to Dicer, they do not act by cleaving dsRNA but
47 rather by inducing a phosphorylation cascade that will ultimately result in the production of the
48 autocrine- and paracrine-acting interferon α and ß cytokines followed by the transcriptional
49 activation of hundreds of interferon stimulated genes (ISGs) (Ivashkiv & Donlin, 2014). Thus,
50 in mammalian somatic cells deficient for MAVS or IFNAR, the production of long-dsRNA-
51 derived siRNAs can be detected and are shown to be dependent on Dicer activity (Maillard *et*
52 *al*, 2016). Besides, the RLR LGP2 has been shown to be directly interacting with Dicer blocking
53 siRNA production and along with TRBP preventing the correct miRNA maturation (Takahashi
54 *et al*, 2018b, 2018a; van der Veen *et al*, 2018). Thus, in mammalian cells RNAi and IFN-I seem
55 to be functionally mutually exclusive and IFN-I is suggested to tone down Dicer involvement
56 in antiviral RNAi.

57 One interesting observation is that the N-terminal helicase domain is quite conserved
58 between RLRs and Dicer, which might indicate a functional replacement during evolution
59 (Baldaccini & Pfeffer, 2021). In mammalian Dicer, the helicase domain exerts some molecular
60 constraints that limit Dicer's processivity for cleaving long dsRNA molecules (Ma *et al*, 2008).
61 Accordingly, a synthetic Dicer lacking the first two domains of the helicase, Hel1 and Hel2i,
62 and named Dicer N1 displays better cleavage properties of an artificial dsRNA than the full-
63 length version of Dicer (Kennedy et al., 2015). More recently, a naturally occurring isoform of
64 Dicer, lacking the Hel2i domain, has been identified in human stem cells and showed to possess
65 some antiviral properties in an RNAi-dependent manner (Poirier *et al*, 2021). Similarly, a Hel1-
66 truncated version of Dicer, coined Dicer^{O}, is specifically expressed in mouse oocytes and is
67 better adapted to cleave long dsRNA molecules than pre-miRNAs (Flemr *et al*, 2013).
68 Uncovering the structure of Dicer^{O} isoform revealed that the N-terminal part of the helicase
69 domain plays an important role for the correct positioning of the pre-miRNA and that removing
70 it potentially increases the affinity for longer dsRNA structures (Zapletal *et al*, 2022). On top
71 of having a molecular self-limiting effect, this helicase domain also allows Dicer to interact
72 with proteins that regulate its activity. We have recently shown that during Sindbis virus (SINV)
73 infection the helicase domain of human Dicer specifically interacts with proteins that are
74 involved in the IFN-I response such as PACT, the RNA helicase DHX9, the adenosine
75 deaminase ADAR1 and the dsRNA-activated protein kinase PKR (Montavon *et al*, 2021). In
76 addition, we reported in the same study that the expression of the helicase-truncated Dicer N1
77 confers a strong antiviral activity against SINV, and that this phenotype is dependent on the
78 presence of PKR. Similarly, another study shows a genetic link between Dicer and PKR in
79 mouse embryonic stem cells and proposes that Dicer can hinder PKR activity in a non-canonical
80 manner (Gurung *et al*, 2021). Dicer thus seems to have an additional antiviral activity linked to
81 PKR that is limited by its helicase domain.

82 In this study, we sought to uncover the mechanism underlying Dicer N1 antiviral
83 activity. By using HEK293T NoDice cells (Bogerd *et al*, 2014) stably expressing either Dicer
84 WT or N1, we showed that Dicer N1 cells are more resistant than Dicer WT cells to infection
85 with alphaviruses SINV and Semliki forest virus (SFV), and human enterovirus 71 (HEV71).
86 However, this antiviral effect was virus-dependent, as Dicer N1 had no impact on vesicular
87 stomatitis virus (VSV) infection, and we even observed a pro-viral effect of Dicer N1 on SARS-
88 CoV-2 infection. Interestingly, we found that the antiviral effect of Dicer N1 is RNAi-
89 independent, as cells expressing a catalytically inactive Dicer N1 were equally protected against
90 SINV infection. We also tested other helicase-truncated mutants of Dicer and observed that
91 individual deletion of each subdomain (Hel1, Hel2i or Hel2) also conferred an antiviral property
92 to Dicer. However, as opposed to Dicer N1, this phenotype appeared to be partially due to
93 RNAi. Nevertheless, all of the helicase-deletion mutants also required the presence of PKR to
94 maintain their antiviral effect. We thus focused our investigations on the implication of PKR in
95 the phenotype of Dicer N1 and showed that it is required for its antiviral activity independently
96 from its kinase function. Transcriptomic analysis of mock- or SINV-infected cells uncovered
97 that Dicer N1 expressing cells have a higher basal expression of a large subset of genes,
98 including a number that are involved in the antiviral response. We further show that those genes
99 are under the control of transcription factors such as STAT1, STAT2 and NF-kB/p65. Finally,
100 we confirmed the importance of the latter pathway in the phenotype of Dicer N1 cells by
101 alleviating the antiviral effect in cells treated with a chemical inhibitor of NF-kB. Based on
102 these results, we propose that one reason for human Dicer to have maintained a self-limiting
103 helicase domain is to prevent basal activation of antiviral and inflammatory pathways.
104

105 **RESULTS**

106 **Effect of Dicer N1 expression on SINV viral cycle**

107 We previously showed that a partial helicase-deletion mutant of human Dicer expressed in
108 HEK293T NoDice cells presented an antiviral activity against SINV (Montavon *et al*, 2021).
109 We used the two monoclonal cell lines NoDice FHA-Dicer WT #4 and NoDice FHA:Dicer N1
110 #6 (afterward respectively referred to as Dicer WT and Dicer N1 cells) to better characterize
111 the impact of Dicer WT or Dicer N1 expression on SINV cycle. We used a non-modified SINV
112 strain and two different GFP-expressing strains that either express the fluorescent protein from
113 a duplication of the subgenomic promoter (SINV-GFP) or from a fusion with the capsid protein
114 (SINV-2A-GFP) (Thomas et al., 2003), the latter expressing GFP at higher levels than the
115 former (Supp. Fig. 1A). We infected Dicer WT or Dicer N1 cells with increasing MOIs of all
116 three viruses and measured the accumulation of infectious particles by plaque assay 24 hours
117 post-infection (hpi) (Fig. 1A). For all viruses, we observed a significant antiviral effect at every
118 MOI in cells expressing Dicer N1 compared to cells expressing Dicer WT. The effect was more
119 pronounced in cells infected with the SINV-2A-GFP, which seems to be attenuated at lower
120 MOIs compared to the two other viral strains (Fig. 1A). We also monitored viral protein
121 accumulation as well as PKR activation in cells infected for 24h at an MOI of 0.02. In Dicer
122 N1 cells, both the Capsid and GFP proteins accumulated to lower levels, or even below
123 detection limits for SINV-2A-GFP, compared to Dicer WT cells (Fig. 1B). PKR
124 phosphorylation could be detected to roughly similar levels in Dicer WT and N1 cells infected
125 with SINV or SINV-GFP. However, it was only detectable in Dicer WT cells but not in Dicer
126 N1 cells, infected with the SINV-2A-GFP, which reflected the attenuation of this virus
127 compared to the two others (Fig. 1B). We also monitored double-stranded (ds) RNA
128 accumulation during infection as a proxy for viral replication. We used the dsRNA-specific J2
129 antibody (Richardson *et al*, 2010) to perform immunostaining of cells infected for 24h at an

130 MOI of 0.02 with either of the three SINV strains. Compared to Dicer WT cells, dsRNA
131 accumulation decreased in Dicer N1 cells for all three viruses, with a stronger effect for the
132 SINV-2A-GFP virus (Fig. 1C). Finally, to further confirm the impact of Dicer N1 expression
133 on viral replication, we finally measured the accumulation of genomic RNA by RT-qPCR in
134 cells infected with SINV-GFP at an MOI of 0.02 for 24h. In agreement with the previous results,
135 Dicer N1 cells showed a very strong decrease of SINV genomic RNA accumulation compared
136 to Dicer WT cells (Fig. 1D). In parallel, we also performed semi-quantitative strand-specific
137 RT-PCR on the same samples and observed that the anti-genomic viral RNA accumulated to
138 lower levels in Dicer N1 cells than in Dicer WT cells. (Supp. Fig. 1B). Collectively, these data
139 indicate that the antiviral activity of Dicer N1 leads to a defect in SINV viral replication.
140

141 **Dicer N1 is antiviral against other positive-strand RNA viruses**

142 To see whether the antiviral activity of Dicer N1 could be generalized to other viruses, we
143 infected Dicer WT and Dicer N1 cells with viruses from different families. We first tested
144 another *Togaviridae*, Semliki forest virus (SFV), and observed a lower viral titer in the
145 supernatants of Dicer N1 cells than in Dicer WT cells infected for 24h at an MOI of 1.10^{-4} (Fig.
146 2A, top panel). In addition, dsRNA accumulation, as assessed by J2 immunostaining, was
147 barely detectable in Dicer N1 cells, whereas it was very high in Dicer WT cells (Fig. 2A, bottom
148 panel). We then infected Dicer WT and N1 cells at an MOI of 0.1 with a (+) RNA virus from
149 the *Picornaviridae* family, human enterovirus 71 (EV71), and measured viral titer in the
150 supernatant by TCID50 at 24 hpi. We observed that the EV71 titer was again lower in Dicer
151 N1 compared to WT cells (Fig. 2B, top panel). J2 immunostaining also confirmed a lower
152 accumulation of dsRNA in Dicer N1 cells compared to WT cells (Fig. 2B, bottom panel). We
153 also tested the effect of Dicer N1 on a single-stranded negative-sense RNA virus from the
154 *Rhabdoviridae* family, *i.e.* vesicular stomatitis virus (VSV). We infected Dicer WT and N1

155 cells at an MOI of 1.10^{-5} for 24h with an engineered VSV expressing the GFP protein and
156 titrated the virus in the supernatant by plaque assay. We did not detect any significant difference
157 in viral titers between Dicer WT and N1 cells (Fig. 2C, top panel). As previously reported
158 (Weber *et al*, 2006), we were not able to detect dsRNA accumulation by J2 immunostaining, in
159 either Dicer WT or N1 cells infected with VSV-GFP. Since dsRNA is a canonical Dicer
160 substrate upon infection, this result indicates that the absence of dsRNA during VSV infection
161 might prevent the activation and antiviral activity of Dicer N1.

162 Finally, we infected the two cell lines with the single-stranded positive-sense RNA virus
163 Severe Acute Respiratory Syndrome Coronavirus 2 (SARS-CoV-2). In order to be able to use
164 this virus in the HEK293T cells we work with, we first transduced them with a lentiviral vector
165 expressing human ACE2 (hACE2), which is an essential receptor for SARS-CoV-2 infection
166 (Hoffmann *et al*, 2020). We verified hACE2 expression by western blot with a specific antibody
167 (Fig. 2D). We infected both hACE2-expressing Dicer WT and Dicer N1 cells with SARS-CoV-
168 2 at an MOI of 1.10^{-3} for 48h, and measured viral nucleocapsid expression by western blot
169 analysis. Nucleocapsid expression could be detected in both Dicer WT and N1 cells and seemed
170 to be slightly higher in the latter (Fig. 2E). We also monitored PKR phosphorylation in this
171 experiment and observed a higher signal in Dicer N1 compared to WT cells. Then, we measured
172 viral titer in the supernatant by TCID50 at 48 hpi. We observed that the SARS-CoV-2 titer was
173 higher in Dicer N1 compared to WT cells (Fig. 2F). We also performed J2 immunostaining on
174 SARS-CoV-2 infected cells, and saw that dsRNA was detected equally well in both Dicer WT
175 and N1 cells (Fig. 2G). Finally, we also measured viral RNA accumulation by RT-qPCR, and
176 saw that both ORF1a and Spike RNAs accumulated to higher levels in Dicer N1 than in Dicer
177 WT cells, although the increase was not significant for Spike RNA (Fig. 2H).

178 Altogether, these last results suggest that Dicer N1 expression can have an antiviral effect
179 for two different (+) RNA viruses (SFV and EV71), but not for a third one (SARS-CoV-2).

180 This antiviral property does not seem to be active in the case of a (-) RNA virus, VSV, which
181 might be related in this case to the difference in dsRNA accessibility.
182
183 **RNA interference is not involved in Dicer N1 phenotype**
184 We showed that Dicer N1 expression prevents the accumulation of viral genomic and
185 antigenomic RNA during SINV infection and of dsRNA during SINV, SFV and EV71
186 infection. Since it was previously shown that Dicer N1 was more active than Dicer WT to cleave
187 an artificial dsRNA into siRNAs (Kennedy et al., 2015), we first hypothesized that the
188 ribonuclease activity of Dicer N1 was responsible for its antiviral activity. To test this
189 hypothesis, we therefore used an affinity-based purification approach (Hauptmann *et al*, 2015)
190 to isolate Ago-associated small RNAs from Dicer WT or N1 cells infected with SINV-GFP at
191 an MOI of 0.02 for 24h and deep-sequenced them. We first mapped the reads to the human and
192 SINV-GFP genomes and observed that the vast majority of small RNAs had a cellular origin
193 (Supp. Fig. 2A). Only 0.2 to 1.2% of sequences could be mapped to the viral genome.
194 Interestingly, the percentage of viral reads was four-to-five-fold lower in Dicer N1 cells than in
195 WT cells. We further analyzed the viral reads and determined their size distribution. Small
196 RNAs mapped to both the genomic and to the antigenomic RNA, with a bias in favor of the
197 former, and showed a peak at 22 nt, consistent with a Dicer-mediated cleavage (Fig. 3A, Supp.
198 Fig. 2B). However, there was no real difference in size distribution or strand origin between
199 Dicer WT and N1 cells. Mapping the small RNAs to the viral genome showed a strong
200 enrichment at the 5' extremity of the genomic RNA in both Dicer WT and N1 cells (Fig. 3B,
201 Supp. Fig. 2C), in agreement with previous reports (Kong *et al*, 2023; Zhang *et al*, 2021). The
202 number of reads that mapped to both strands of the viral RNA was however higher in Dicer
203 WT than in N1 cells. It therefore appears that both Dicer WT and Dicer N1 are competent for
204 the generation of what looks like viral siRNAs that are loaded in Argonaute proteins, but we

205 did not see an increase in their number in Dicer N1 expressing cells. At this stage, we therefore
206 cannot say that the observed antiviral phenotype of Dicer N1 is linked to a stronger RNAi
207 activity.

208 To further confirm that the Dicer N1 phenotype was independent of its role in RNAi, we
209 generated a catalytic-deficient version of Dicer N1 by introducing mutations in both of its
210 RNAse III domains (Fig. 3C). As previously, we used the HEK293T NoDice 2.20 cell line
211 (Bogerd *et al*, 2014) that we transduced with lentiviral vectors expressing a Flag-HA-tagged
212 version of Dicer N1 with mutations in the catalytic domain (N1-CM). We then selected a clone,
213 NoDice FHA:Dicer N1-CM #2.17 (afterwards called Dicer N1-CM), that expressed Dicer at
214 levels similar to the Dicer WT and Dicer N1 cell lines previously generated (Fig. 3D). The
215 levels of PKR and TRBP were mostly similar to the ones in Dicer N1 cells. By blotting AGO2
216 expression in these cell lines, we observed that it was absent in the Dicer N1-CM cells, which
217 is expected for a miRNA-free Argonaute protein and is consistent with previous observations
218 (Gibbings *et al*, 2012). We confirmed the defect in miRNA processing in the Dicer N1-CM
219 cells by measuring miR-16 accumulation by northern blot analysis. As expected, we saw no
220 mature miR-16 form and the accumulation of its precursor in Dicer N1-CM cells (Fig. 3E). We
221 then infected Dicer WT, N1 and N1-CM cells with SINV-GFP at an MOI of 0.02 for 24h and
222 measured the infection rate by western blot analysis and plaque assay. The level of the capsid
223 protein was strongly reduced in both Dicer N1 and Dicer N1-CM cells compared to Dicer WT
224 cells (Fig. 3F). In addition, we could not detect PKR or eIF2α phosphorylation in neither Dicer
225 N1 nor Dicer N1-CM cells. To confirm these observations, we titrated the infectious viral
226 particles in the supernatant and observed a strong and significant decrease of viral titers in both
227 Dicer N1 and Dicer N1-CM compared to Dicer WT cells (Fig. 3G). To rule out any clone-
228 dependent effect, we performed the same experiment in polyclonal cells expressing Dicer WT,
229 N1 or N1-CM. As for the monoclonal cell lines, Dicer N1 and N1-CM cells displayed a drop

230 in Capsid protein accumulation and an absence of PKR activation compared to Dicer WT cells
231 (Supp. Fig. 2D). Accordingly, the viral titer was strongly reduced in Dicer N1 and N1-CM cells
232 compared to Dicer WT cells (Supp. Fig. 2E). We showed previously that Dicer N1 could no
233 longer interact with the Dicer co-factors TRBP and PACT and with the kinase PKR (Montavon
234 *et al*, 2021). Thus, we verified by co-immunoprecipitation the interaction of Dicer N1-CM with
235 these proteins. The results confirmed that Dicer N1-CM behaved similarly to Dicer N1
236 regarding the loss of these interactions (Supp. Fig. 2F).
237 Taken together, these results clearly show that the antiviral phenotype of Dicer N1 does
238 not depend on its catalytic activity, and therefore on RNAi, which is in agreement with our
239 previous observations that the antiviral effect of Dicer N1 did not depend on AGO2 (Montavon
240 *et al*, 2021).
241
242 **Impact of Dicer helicase subdomain deletions on viral infection**
243 The region deleted in Dicer N1 contains both the Hel1 and Hel2i domains of the helicase, and
244 was designed based on the presence of an alternative initiation codon at this position (Kennedy
245 et al., 2015). Other deletion mutants have been reported in the literature, such as the rodent-
246 specific Dicer^{O}, which is naturally expressed in oocytes (Flemr *et al*, 2013). Similar to Dicer
247 N1, this truncated Dicer was shown to be more potent at generating siRNAs, and was further
248 functionally and structurally studied under the name Dicer ΔHel1 (Zapletal *et al*, 2022). Finally,
249 another Dicer isoform has been recently reported in human embryonic stem cells and was
250 coined antiviral Dicer (AviD) for its RNAi-related antiviral property against different viruses
251 (Poirier *et al*, 2021). This isoform lacks the Hel2i connector domain. To test the behavior of all
252 these deletion mutants during SINV infection, we generated lentiviral constructs expressing a
253 Flag-HA tagged version of Dicer ΔHel1, ΔHel2i and a version lacking the third helicase domain
254 ΔHel2 (Fig. 4A). We used these lentiviral constructs, as well as catalytically inactive version

255 of them called CM, to generate monoclonal NoDice cell lines. We first verified the correct
256 expression of the Dicer isoforms and checked their impact on AGO2, TRBP, PACT and PKR
257 expression (Supp. Fig. 3A). We also checked that the catalytically inactive versions of the
258 constructs were indeed impaired in miRNA biogenesis by measuring miR-16 expression by
259 northern blot analysis (Supp. Fig. 3B). We then infected cells expressing Dicer WT, ΔHel1,
260 ΔHel2i, ΔHel2 or their catalytically inactive versions (CM) with SINV-GFP at an MOI of 0.02
261 for 24h and monitored Capsid protein accumulation by western blot analysis. The levels of
262 Capsid were lower in all cell lines expressing helicase truncated versions of Dicer compared to
263 Dicer WT cells, but seemed to go up when the RNAse III activity was mutated, although slightly
264 less so in the case of ΔHel2 (Fig. 4B). To really assess the impact of the expression of these
265 mutants on viral production, we titrated by plaque assay the supernatants of the previous
266 experiment, using Dicer N1 cells as control. We observed that expression of all helicase
267 deletion mutants, Dicer ΔHel1, ΔHel2i and ΔHel2, resulted in a significant drop in viral titer,
268 although slightly less than in Dicer N1 expressing cells, and that this effect was lost in cells
269 expressing the CM versions of the mutants (Fig. 4C). Altogether, these results suggest that
270 deleting any helicase subdomain confers an antiviral activity to human Dicer.

271 We previously showed that Dicer N1 antiviral phenotype was dependent on the
272 expression of PKR (Montavon *et al*, 2021). We therefore tested the impact of the expression of
273 the various helicase deletion mutants on viral infection in NoDice compared to NoDiceΔPKR
274 cells. We transduced the aforementioned cell lines with Dicer WT, N1, ΔHel1, ΔHel2i and
275 ΔHel2 to generate polyclonal cell lines. We again made sure that these cell lines expressed the
276 different Dicer constructs, that they expressed similar levels of interacting proteins such as
277 AGO2, TRBP and PACT (Supp. Fig. 3C), and that they were also competent for miRNA
278 production (Supp. Fig. 3D). We then infected all those cell lines with SINV-GFP at an MOI of
279 0.02 for 24h and measured the expression of the Capsid protein by western blot analysis. We

280 could observe a lower accumulation in NoDice cells transduced with Dicer ΔHel1, ΔHel2 and
281 ΔHel2i compared to cells transduced with Dicer WT (Fig. 4D), although the effect was less
282 evident for cells expressing Dicer ΔHel2. On the contrary, in NoDiceΔPKR cells transduced
283 with Dicer ΔHel1, ΔHel2 and ΔHel2i, we did not observe such a strong decrease in Capsid
284 protein levels. We then determined the viral titers produced upon SINV-GFP infection of
285 NoDice or NoDiceΔPKR cells expressing Dicer WT, N1, ΔHel1, ΔHel2i or ΔHel2. While we
286 confirmed the antiviral effect of the helicase deletion mutants compared to the WT Dicer in
287 NoDice cells, we saw that this effect was completely abrogated in NoDiceΔPKR cells (Fig.
288 4E). We can therefore conclude that the antiviral phenotype of Dicer N1 can also be observed
289 with smaller deletion mutants lacking individual subdomains of the helicase. However, as
290 opposed to Dicer N1, it seems that in the case of Dicer ΔHel1, ΔHel2i or ΔHel2, this phenotype
291 is dependent on the catalytic activity of Dicer, and thus is likely RNAi-dependent. Yet, the
292 phenotype is also lost in cells that do not express PKR, a property which is also seen with Dicer
293 N1. We thus decided to look more into the role of PKR.
294
295 **PKR, but not its catalytic activity, is directly involved in the Dicer N1 antiviral phenotype**
296 As shown above, the antiviral phenotype of Dicer helicase mutants seems to be strictly
297 dependent on the expression of PKR. To validate the implication of PKR, we decided to re-
298 express it in NoDiceΔPKR cells to see whether this would complement the antiviral phenotype
299 of Dicer N1. We also designed mutant versions of PKR as indicated in Figure 5A. These
300 mutants are: K296R, which is not able to bind ATP, homodimerize, autophosphorylate or
301 phosphorylate its targets (Dey *et al*, 2005), and T451A, which is still able to form homodimers
302 but loses its ability to autophosphorylate the T451 residue and to phosphorylate its targets
303 (Taylor *et al*, 2001). We first transduced constructs expressing a MYC:CTRL, MYC:PKR WT,
304 MYC:PKR K296R or MYC:PKR T451A in NoDiceΔPKR FHA:Dicer WT cells and infected

305 them with SINV-GFP at an MOI of 0.02 for 24h. We analyzed the expression of PKR and its
306 phosphorylated form by western blot analysis, which confirmed that all constructs were
307 expressed at high levels, but only WT PKR could be phosphorylated upon SINV infection (Fig.
308 5B). Interestingly, there was some basal level of phosphorylated PKR in the mock-infected
309 cells expressing WT PKR, which could be due to a higher expression of PKR in transduced
310 cells compared to WT cells. The activation of the MYC:PKR WT construct in the infected
311 condition resulted in an increase in eiF2α phosphorylation compared to the CTRL or mutant
312 PKR constructs. Even in the absence of PKR or in the presence of catalytically inactive version
313 of it, some levels of eiF2α phosphorylation could be detected in the SINV-infected conditions,
314 probably due to the activity of the GCN2 kinase as previously reported (Berlanga *et al*, 2006).
315 In terms of viral capsid accumulation, no real difference could be detected between the different
316 conditions (Fig. 5B). We measured viral particles production by plaque assay in SINV-GFP
317 infected cells, and could not detect any difference between samples (Fig. 5C). This result
318 indicates that in the presence of Dicer WT, expression of a WT or inactive mutant PKR has no
319 significant impact on SINV infection. We then transduced the same MYC:CTRL or PKR
320 constructs as above in NoDiceΔPKR FHA:Dicer N1 cells and performed the same analysis after
321 infection with SINV-GFP. The western blot analysis was consistent with the previous one and
322 confirmed the correct expression of the PKR constructs as well as activation of only the WT
323 PKR version (Fig. 5D). However, we noted a small reduction of Capsid protein accumulation
324 in cells expressing MYC:PKR WT, K296R or T451A compared to the MYC:CTRL condition
325 (Fig. 5D). This was confirmed by the plaque assay analysis that revealed a significant drop in
326 viral titer in NoDiceΔPKR Dicer N1 cells expressing WT or inactive PKR compared to cells
327 expressing the negative control (Fig. 5E). We could thus restore the antiviral phenotype of Dicer
328 N1 by re-expressing PKR in cells where its expression was ablated. Interestingly, this did not
329 require a catalytically active or homodimerization competent PKR since the same

330 complementation could be observed with two different mutants that were both unable to
331 phosphorylate their substrates. Overall, these results suggest that the antiviral activity of Dicer
332 N1 is linked to PKR, but does not require the canonical activation of PKR through
333 homodimerization and phosphorylation.
334
335 **Expression of Dicer N1 induces major changes in the transcriptome**
336 To decipher the mechanism behind Dicer N1 antiviral property, we performed total RNAseq
337 analysis on both Dicer WT and Dicer N1 cells either mock-infected, infected with SINV-GFP
338 at an MOI of 2 for 12h or infected with SINV-GFP at an MOI of 0.02 for 24h. We first verified
339 the percentage of viral reads in the libraries and observed that it was higher (about 8-fold for
340 the genomic RNA) in Dicer WT than in Dicer N1 cells (Supp. Fig. 4A). This confirmed the
341 antiviral effect of Dicer N1 at the level of viral replication. Next, we compared the overall
342 profiles of gene expression in the different conditions (Fig. 6A). The analysis identified 5
343 groups of genes according to their expression patterns. The first group was composed of genes
344 overexpressed in N1 cells compared to WT cells. The second one was composed of genes
345 specifically downregulated in WT cells upon infection, whereas the third one represented genes
346 downregulated upon infection in both cell lines. Finally, the fourth and fifth groups comprised
347 genes that are upregulated in both WT and N1 cells or in WT cells only, respectively. The first
348 two groups were of interest as several genes were upregulated in Dicer N1 cells no matter
349 whether there were infected or not. We then performed a differential gene expression analysis
350 of mRNAs using DEseq2 (Love *et al*, 2014) to determine the impact of the infection on the cell
351 transcriptome. The results confirmed that in Dicer WT cells, infection by SINV resulted in
352 major changes in the expression levels of a large number of mRNAs, which were visible both
353 at 12 and 24 hpi (Fig. 6B, Supp. Fig. 4B). However, in Dicer N1 cells, these changes were
354 substantially more limited at both time points of infection (Fig. 6C, Supp. Fig. 4B), consistent

355 with the fact that the infection was attenuated in these cells and therefore did not result in a
356 strong cellular response. Strikingly, when we compared the transcriptomes of mock-infected
357 Dicer WT and Dicer N1 cells, we found that there was a large number of up-regulated mRNAs,
358 as well as a smaller number of down-regulated mRNAs (Fig. 6D). It seems therefore that the
359 expression of Dicer N1 results in changes at the transcriptional level, so we set out to examine
360 whether any of these perturbations could explain the phenotype we observed in these cells. To
361 better characterize the phenotypical dynamics underlying differentially expressed genes
362 (DEGs), we looked at gene set enrichment analysis (GSEA) against the Hallmark biological
363 states and processes gene sets (Fig. 6E, Supp. Fig. 4C, D). In Dicer N1 cells, processes linked
364 to interferon alpha and gamma, and to inflammatory and NF-kB responses were significantly
365 enriched (Fig. 6E). Interestingly, the interferon alpha and gamma pathways were already
366 enriched in mock cells, whereas those pathways were not enriched in WT cells upon SINV
367 infection. This was confirmed by the increased number of genes linked to interferon and
368 inflammatory pathways in Dicer N1 cells compared to WT cells, denoting a basal IFN-I
369 signature linked to a subset of genes in N1 cells (Supp. Fig. 4C). Conversely, those pathways
370 were not detected in WT cells upon infection (Supp. Fig. 4D).
371 Altogether, these results highlight transcriptomic differences in Dicer N1 compared to
372 WT cells in mock and SINV infected cells. Globally, immune-related pathways seem to be
373 enriched in Dicer N1 cells, and this, even in the steady state.
374
375 **Dicer N1 expression increases the activation of immune-related transcription factors**
376 Given the seemingly increased RNA Pol II transcription in the Dicer N1 cells, we looked
377 for transcription factors that are known to play important roles in innate immunity and analyzed
378 the expression levels of their target genes in the different samples. We retrieved the known
379 targets of NF-kB/p65, STAT1, STAT2, IRF2 and IRF3 and extracted from these lists genes that

380 were differentially expressed either during infection in Dicer WT or Dicer N1 cells, or between
381 mock-infected Dicer WT and Dicer N1 cells. We then computed the cumulative frequencies of
382 de-regulated transcripts by comparing i) Dicer WT SINV-GFP 24hpi vs. Dicer WT Mock, ii)
383 Dicer N1 SINV-GFP 24hpi vs. Dicer N1 Mock and iii) Dicer N1 Mock vs. Dicer WT Mock.
384 This calculation was done for NF-kB/p65 (Fig. 7A) and STAT2 (Fig. 7B), which were the ones
385 with the greater changes, but also for IRF2 (Supp. Fig. 5A), IRF3 (Supp. Fig. 5B) and STAT1
386 (Supp. Fig. 5C). The results indicate first that when comparing Dicer WT SINV-infected vs.
387 Mock and Dicer N1 SINV-infected vs. Mock, there were more target genes either up or down-
388 regulated in the Dicer WT cells than in the Dicer N1 cells, which again reflects the lower
389 response of Dicer N1 cells to the infection. Surprisingly, there were significantly more
390 upregulated transcripts when comparing Dicer N1 Mock to Dicer WT Mock than when
391 comparing Dicer WT SINV-infected to Dicer WT Mock conditions (see the red vs. black curves
392 in Fig. 7A, B). A global representation in the form of heatmaps for the same set of genes that
393 are known targets of NF-kB/p65 or STAT2 also allowed to visualize the stronger changes
394 induced by the infection in Dicer WT cells compared to Dicer N1 cells, and that a number of
395 transcripts were more expressed in Dicer N1 Mock than in Dicer WT Mock condition (Fig. 7C,
396 D). We also represented DEseq2 data on volcano plots for NF-kB/p65 and STAT2 for the Dicer
397 WT infected vs mock and Dicer N1 mock vs Dicer WT mock comparisons (Supp. Fig. 5D, E).
398 As seen previously, genes under the control of NF-kB and STAT2 appeared to be more
399 upregulated in Dicer N1 mock cells than in WT cells either mock or SINV-infected.
400 We validated the increased expression of some selected target genes by RT-qPCR and
401 could confirm that PTGS2, APOBEC3B, MX1, OAS3, and IFIT3 mRNAs were indeed
402 significantly upregulated in mock-infected Dicer N1 compared to Dicer WT cells (Fig. 7E).
403 Conversely, very mild or no expression increase and sometimes a decrease in expression was
404 detected for the selected target genes in Dicer N1 infected compared to mock cells, consistent

405 with the RNAseq analysis (Supp. Fig. 5F). Besides, the expression decrease observed in WT
406 cells upon infection was expected as SINV blocks RNA Pol II transcription via its nsP2 protein
407 (Akhrymuk *et al*, 2018).

408 Overall, the transcriptome changes induced by Dicer N1 expression, which we validated
409 for selected transcripts by RT-qPCR, allow us to postulate that these cells are in a pre-activated
410 state that might explain their increased resistance to SINV infection.

411

412 **The NF-kB pathway is implicated in the antiviral phenotype of Dicer-N1**

413 We showed above that the presence of PKR but not its canonical kinase activity was needed for
414 the Dicer N1 antiviral phenotype. It has been reported that PKR can be involved in activating
415 the immune response in a non-canonical manner. In particular, PKR has been described as an
416 inducer of NF-kB/p65 transcriptional activity independently of its kinase function (Bonnet *et*
417 *al*, 2000). Since we also found that targets of NF-kB are induced specifically in Dicer N1 cells,
418 we investigated whether this pathway was involved in the antiviral phenotype of these cells.
419 NF-kB/p65 is known to be phosphorylated once IkBα is released from the complex, which
420 results in NF-kB/p65 activation upon translocation into the nucleus (Christian *et al*, 2016;
421 Kanarek & Ben-Neriah, 2012). We looked at the expression and phosphorylation levels of NF-
422 kB/p65 in Dicer WT and N1 cells during a time course of SINV-GFP infection at an MOI of 2
423 from 3 to 24 hpi (Fig. 8A). In Dicer WT cells, we observed an increase in p65 phosphorylation
424 at 6 hpi, which corresponds to the end of the first replication cycle. However, at 12 hpi the
425 phosphorylation decreased and became undetectable at 24 hpi. In Dicer N1 cells, the level of
426 phosphorylated p65 was already quite elevated in the mock-infected condition and remained
427 high, independently of PKR phosphorylation, until 12 hpi where it slightly decreased until 24
428 hpi (Fig. 8A). At the same time, we noticed a higher level of NF-kB/p65 protein at both 12 and
429 24 hpi.

430 Given the higher activation levels of p65 in Dicer N1 cells, we then decided to block the
431 NF-kB pathway to test its role during SINV infection. To do so, we used the chemical
432 compound BAY 11-7082, which inhibits IkBα phosphorylation by the IKK kinases and thus
433 prevents NF-kB/p65 activation (Pierce *et al*, 1997). We treated Dicer N1 cells with two
434 different concentrations of BAY 11-7082 during 1h. Then, we infected cells with SINV-GFP
435 at an MOI of 0.02 for 24h and evaluated the impact of the drug treatment on the infection
436 efficiency. As shown in Figure 8B (top panel), we observed a decrease in the phosphorylation
437 of p65 in mock-infected cells treated with 5 µM of BAY 11-7082 compound compared to cells
438 treated with DMSO only. Conversely, the level of IkBα was increased in cells treated with the
439 inhibitor compared to the control (Fig. 8B, lower panel). These results indicate that the
440 treatment was effective. We further validated that the inhibitor worked as expected by analyzing
441 the levels of one of the previously validated NF-kB target mRNAs, PTGS2, by RT-qPCR. In
442 Dicer N1 cells treated with 5 µM of BAY 11-7082, the level of this mRNA was significantly
443 reduced compared to the control condition (Fig. 8C). The effect of the NF-kB inhibitor on viral
444 infection could be visualized first by the increased detection of the Capsid protein in SINV-
445 GFP infected cells treated with 5 µM of BAY 11-7082 compared to DMSO-treated cells (Fig.
446 8B). Finally, we measured the effect of NF-kB inhibition on viral particles production, and
447 observed a significant increase in viral titers in Dicer N1 cells treated with 5µM of BAY
448 compared to the negative control (Fig. 8C). The BAY 11-7082 treatment had no effect on
449 SINV-GFP infection in Dicer WT cells, as assessed by western blot analysis of the Capsid
450 protein and by plaque assay (Supp. Fig. 6A, B). Overall, these results indicated that by blocking
451 the NF-kB/p65 pathway with BAY 11-7082, the antiviral activity of Dicer N1 could be
452 reverted, suggesting that the antiviral activity of Dicer N1 is partially mediated through the NF-
453 kB/p65 pathway.
454

455 **DISCUSSION**

456 In this study, we examined the role played by Dicer during viral infection in human cells. We
457 specifically focused on the importance of its helicase domain, as it is known to play important
458 roles in modulating its activity. Indeed, some of the deletion mutants that we used in our
459 analysis, such as Dicer N1, Dicer ΔHel1 or Dicer ΔHel2i have been reported to display an
460 increased RNAi activity either directed against artificial dsRNA substrate or specific viruses
461 (Kennedy et al., 2015; Poirier et al., 2021; Zapletal et al., 2022). Our results confirmed that
462 helicase-truncated Dicer proteins displayed an antiviral phenotype against some, but not all,
463 viruses. While we observed that the catalytic activity of Dicer was involved for some deletion
464 mutants, we also showed that the presence of the PKR protein was an essential feature for this
465 phenotype. In particular, the Dicer N1 variant, which was shown to be capable of RNAi activity
466 in cells that did not express PKR (Kennedy et al., 2015) was in our hands antiviral only in the
467 presence of PKR, and remained antiviral when rendered catalytically inactive. A link between
468 Dicer and PKR was also proposed in mouse embryonic stem cells where Dicer appears to
469 prevent the PKR-induced IFN-I response (Gurung *et al*, 2021). However, no mechanism was
470 proposed, and the authors hypothesized that it might be linked to miRNA production. Our data
471 seem to indicate that the PKR-mediated antiviral effect observed in cells expressing helicase-
472 truncated Dicer proteins is dominant over the RNAi-mediated effect. One would expect that
473 RNAi would be more potent when PKR is not expressed since it should compete with Dicer for
474 dsRNA binding. The fact that it is not the case during the antiviral response raises interesting
475 perspectives.

476 PKR is a key effector protein involved in pathways such as apoptosis, autophagy, cell
477 cycle control and immunity (Williams, 1999). Besides its well-known role in translation control
478 *via* phosphorylation of the eIF2α factor (Donnelly *et al*, 2013) it also plays key roles in
479 modulating IFN-I signaling pathways and can negatively regulate STAT1 and STAT3

480 transcriptional activity in a kinase-dependent manner (Raven *et al*, 2006). It has also been
481 involved in the NF-kB pathway, but in this case it can do so both in a catalytic-dependent (Gil
482 *et al*, 2001) and independent way, via the IKK kinase (Bonnet *et al*, 2000; Ishii *et al*, 2001).
483 Here, we showed that Dicer N1 expressing cells had a different transcriptome from Dicer WT
484 expressing cells and that the differentially expressed genes are mostly involved in the interferon
485 alpha/gamma and inflammatory/NF-kB pathways. Specifically, we could identify among those
486 a substantial fraction of targets of key immune transcription factors such as STAT2 and NF-
487 kB. We retrieved and validated the differential expression levels for known antiviral effectors
488 such as PTGS2, APOBEC3B or OAS3 (Jiang *et al*, 2008; Lehman *et al*, 2022; Manjunath *et al*,
489 2023; Ryman *et al*, 2002). This observation is reminiscent of other studies that showed that
490 Dicer could be involved in non-RNAi related signaling pathways. For instance, *Drosophila*
491 Dicer-2 can induce the expression of a small antiviral peptide, Vago, in a tissue- and virus-
492 specific manner (Deddouche *et al*, 2008). More recently, plant DCL2 was involved in auto-
493 immunity activation upon *DCL4* loss and in the activation of defense gene expression such as
494 nucleotide-binding domain/leucine-rich repeat immune receptors (Nielsen *et al*, 2023). We
495 showed that by treating Dicer N1 expressing cells with an NF-kB inhibitor, we could abrogate
496 their antiviral phenotype. We thus partially validated our hypothesis that the transcriptional
497 deregulation of key genes involved in the innate immune response was responsible for the
498 observed effect on virus infection. Furthermore, the fact that Dicer N1 cells were not protected
499 against SARS-CoV-2 infection is also in favor of an involvement of NF-kB or STAT1/2
500 signaling pathways. Indeed, SARS-CoV-2 is known to benefit from the upregulation of the
501 inflammatory response, mainly through the NF-kB pathway, which is essential for the
502 replication and propagation of the virus (Nilsson-Payant *et al*, 2021).

503 Our study reinforces the non-canonical roles of Dicer in immune signaling pathways and
504 its interplay with the IFN-I response. Dicer helicase domain sequesters PKR away from its

505 unconventional signaling function. We showed that Dicer N1 antiviral activity only depends on
506 the presence of PKR but not on its dimerization or catalytic activity. Even though we cannot at
507 this stage formally conclude on the mechanism at play, we can speculate that PKR cofactors
508 TRBP and/or PACT might be involved. Indeed, PKR can be activated by PACT upon stress
509 (Farabaugh *et al*, 2020; Ito *et al*, 1999). Conversely, TRBP can inhibit PKR directly or sequester
510 PACT away from PKR (Chukwurah & Patel, 2018; Daher *et al*, 2009). Since both proteins are
511 also interacting with Dicer, *via* its helicase domain, and thus cannot interact with it anymore in
512 the Dicer N1 cells, they are therefore expected to preferentially interact with other partners such
513 as PKR in the Dicer N1 background and they could limit or change its canonical function. This
514 could in theory explain the activation of the NF-kB pathway in a PKR-dependent manner in the
515 presence of a helicase-truncated Dicer. Interestingly, it was previously shown that the NF-kB
516 pathway could promote SINV infection, but only in mature non-dividing neurons (Yeh *et al*,
517 2019). In the proliferating cell line that we used, we rather showed that the basal activation
518 level of NF-kB in Dicer N1 cells is antiviral. In agreement with this observation, inhibiting NF-
519 kB in Dicer WT cells has no effect on SINV, which is similar to what has been reported in the
520 Yeh et al. study. Our results therefore indicate that in actively dividing cells, the NF-kB status
521 dictates the fate of SINV infection, and this can be in part controlled by the Dicer isoform
522 expressed. This also means that in cells that naturally express isoforms of helicase-truncated
523 Dicer, *i.e.* oocytes and stem cells, it would be important to check whether signaling pathways
524 are deregulated and whether this contributes to the antiviral effect that has been reported for the
525 AviD isoform (Poirier *et al*, 2021).

526 Overall, our study reinforces the idea of a crosstalk between IFN-I and RNAi highlighting
527 a non-canonical function of human Dicer upon infection. We showed that Dicer helicase
528 domain is linked to the prevention of the immune signaling pathway, and can therefore prevent
529 basal activation of this pathway. PKR, free from its interaction with human Dicer, displays an

530 antiviral IFN-I-triggering role against alphaviruses and an enterovirus that is independent from

531 Dicer activity.

532 **MATERIAL & METHODS**

533 **Plasmids, cloning and mutagenesis**

534 N1 DICER, N1-CM DICER, ΔHEL1 DICER and ΔHEL1-CM DICER were generated by PCR
535 mutagenesis from pDONR-DICER described in (Girardi *et al*, 2015). ΔHEL2i and ΔHEL2
536 DICER and their catalytic mutants (CM) were generated by InFusion mutagenesis (Takara Bio)
537 on pDONR-DICER and pDONR-DICER catalytic mutant vectors. pLenti Flag-HA-V5 vector
538 was modified from pLenti6-V5 gateway vector (Thermo Fisher scientific V49610) by Gibson
539 cloning. WT, N1, N1-CM, ΔHEL1, ΔHEL2i, ΔHEL2, ΔHEL1-CM, ΔHEL2i-CM and ΔHEL2-
540 CM DICER from pDONR plasmids were cloned in pLenti flag-HA-V5 by Gateway
541 recombination.

542 pLenti MYC:PKR and pLenti human ACE2 vectors were purchased from VectorBuilder.
543 pLenti MYC:CTRL vector was modified from pLenti MYC:PKR by InFusion cloning (Tanaka
544 Bio). PKR K296R and PKR T451A were obtained by InFusion mutagenesis (Takara Bio) on
545 pLenti MYC:PKR vector.

546 All primers used are listed in Supplementary Table 1.

547

548 **Cell lines**

549 HEK293T, HEK293T/NoDice (2.20), HEK293T/NoDiceΔPKR cell lines were a gift from Pr.
550 Bryan Cullen (Duke University, Durham NC, USA) and described in (Bogerd *et al*, 2014;
551 Kennedy *et al*, 2015). Vero E6 cells were bought at ATCC (CRL-1586).

552

553 **Cell culture and transfection**

554 Cells were maintained in Dulbecco's modified Eagle medium (DMEM, Gibco, Life
555 Technologies) supplemented with 10% fetal bovine serum (FBS, Clontech) in a humidified

556 atmosphere with 5% CO_2 at 37°C. Transfections were performed using Lipofectamine 2000
557 (Invitrogen, Fisher Scientific) according to the manufacturer's instructions.
558
559 **BAY 11-7082 treatment**
560 NoDice FHA:DICER WT #4 and N1 #6 cells were treated with BAY 11-7082 (Merck) by
561 replacing the culture medium with a medium containing the indicated BAY 11-082
562 concentrations at 1µM or 5µM or the corresponding volume of DMSO only in the control
563 conditions. Treatment was maintained for 1h and media was changed with the infection media
564 with SINV-GFP at an MOI of 0.02 for 24h. Proteins, RNA and supernatants were then collected
565 and analyzed.
566
567 **Lentivirus production and generation of stable cell lines**
568 The lentiviral supernatant from single transfer vector was produced by transfecting HEK293T
569 cells with 1.7µg of the transfer vector (either pLenti6 FHA-V5 or pLenti MYC), 0.33 µg of the
570 pVSV envelope plasmid (Addgene #8454) and 1.33µg of pSPAX2 packaging plasmid
571 (Addgene #12260) using Lipofectamine 2000 (Invitrogen, Fisher Scientific) reagent according
572 to the manufacturer's protocol. HEK293T were maintained in DMEM (Gibco, Life
573 Technologies) medium supplemented with 10% Fetal bovine serum (FBS, Clontech). One well
574 from a 6-well-plate at 70% confluency was used for the transfection. The medium was replaced
575 6 hours post-transfection. After 48 hours, the medium containing viral particles was collected
576 and filtered through a 0.45µm PES filter. Different cell lines were transduced: NoDice (for N1,
577 N1-CM, ΔHEL1, ΔHEL1-CM, ΔHEL2i, ΔHEL2i-CM, ΔHEL2 and ΔHEL2-CM),
578 NoDiceΔPKR (for WT, NA, ΔHEL1, ΔHEL1-CM, ΔHEL2i, ΔHEL2i-CM, ΔHEL2 and
579 ΔHEL2-CM), NoDiceΔPKR FHA:CTL or FHA:DICER WT #2 or FHA:DICER N1 #6 (for
580 CTRL, PKR, K296R, T451A), NoDice:FHA DICER WT #4 or N1 #6 (for ACE2). One well of

581 a 6-well-plate was transduced using 500µL of filtered lentiviral supernatant either expressing
582 DICER or PKR or ACE2 constructs, 500µL of DMEM supplemented with 10% FBS and
583 4µg/mL polybrene (Merck, Sigma Aldrich) for 6 hours. Then, the medium was changed with
584 DMEM supplemented with 10% FBS for 24 hours and the resistant cell clones were selected
585 with the right antibiotic and subsequently maintained under the selection. For NoDice, the
586 selection lasted for 2 weeks with blasticidin at 15µg/mL (Invivogen). For NoDiceΔPKR, the
587 selection lasted for 2 weeks with blasticidin at 10µg/mL (Invivogen). For NoDiceΔPKR
588 FHA:CTL or DICER WT #2, the selection lasted 11 days with hygromycin at 100µg/mL and
589 for NoDiceΔPKR FHA:DICER N1 #6 it was the same but with hygromycin at 150µg/mL
590 (Invivogen). Lastly, the ACE2-tranduced cells were selected for 10 days with zeocin at
591 15µg/mL (Invivogen).
592
593 **Viral stocks, virus infection**
594 Viral stocks of SINV WT, SINV-2A-GFP and SINV-GFP were produced as described in
595 (Girardi *et al*, 2015). SINV-2A-GFP was described in (Thomas *et al*, 2003). Cells were infected
596 with SINV (strain AR339), SINV-2A-GFP and SINV-GFP at an MOI of 0.02 or for SINV-GFP
597 at an MOI of 2 and samples were collected at the different indicated time points.
598 Viral stocks of SFV were propagated in Vero E6 cells from the initial stock (strain
599 UVE/SFV/UNK/XX1745; EVAg 001V-02468). Cells were infected at an MOI of 1.10^{-4} for 24
600 hours.
601 Viral stocks of EV71 were produced by one passage in BHK21 cells from the initial stock
602 (ATCC VR-1432). Cells were infected at an MOI of 0.1 for 24 hours.
603 Viral stocks of VSV-GFP were propagated in BHK21 cells from the initial stock (strain Indiana
604 isolate PI10; described in (Mueller *et al*, 2010)). Cells were infected at an MOI of 1.10^{-5} for 24
605 hours.

606 Viral stocks of SARS-CoV-2 were produced by two passages in Vero E6 cells from the initial
607 stock (strain human/DEU/HH-1/2020; EVAg 002V-03991). Cells were infected at an MOI of
608 0.01 or 0.001 for 24 or 48 hours.
609
610 **Analysis of viral titer by plaque assay**
611 For SINV, SINV-2A-GFP and SINV-GFP, Vero E6 cells were seeded in 96-well plates and
612 infected with 10-fold serial dilutions of infection supernatants for 1 hour. The inoculum was
613 removed and cells were covered with 2.5% carboxymethyl cellulose and cultured for 72 hours
614 at 37°C in a humidified atmosphere of 5% CO_2. Plaques were counted manually under the
615 microscope and viral titer was calculated according to the formula: *PFU/mL = #plaques/*
616 *(Dilution*Volume of inoculum).*
617 For SFV and VSV-GFP, Vero E6 cells were seeded in 24-well plates format and were infected
618 with 10-fold serial dilutions of infection supernatants for 1 hour. The inoculum was removed
619 and cells were covered with 2.5% carboxymethyl cellulose and cultured for 48 hours at 37°C
620 in a humidified atmosphere with 5% CO_2. For plaques visualization, the carboxymethyl
621 cellulose was removed. Cells were fixed with 4% formaldehyde (Merck, Sigma Aldrich) in
622 PBS (phosphate buffered saline, Gibco) for 20 minutes at room temperature (RT). Cells were
623 then stained with a 1X crystal violet solution for 20 minutes at RT (2% crystal violet, Sigma;
624 20% ethanol; 4% formaldehyde, Merck). Plates were washed with clear water and plaques were
625 counted manually. The viral titer was calculated according to the formula: *PFU/mL = #plaques/*
626 *(Dilution*Volume of inoculum).*
627
628 **Analysis of viral titer by TCID50**
629 For EV71 and SARS-CoV-2, Vero E6 cells were seeded in 96-well plates already containing
630 10-fold serial dilutions of infection supernatants. Cells were maintained three to four days at

631 37°C in a humidified atmosphere with 5% CO_2. Wells containing dead cells were counted
632 manually under the microscope and viral titer was calculated according the Spearman-Kaerber
633 50% lethal dose formula described in (Wilham *et al*, 2010; Wulff *et al*, 2012).
634
635 **Western blot analysis**
636 Proteins were extracted and homogenized in the appropriate volume of ice-cold lysis buffer
637 (50mM Tris-HCl pH 7.5, 5mM EDTA, 150mM NaCl, 0.05% SDS, 1% Triton X-100 and
638 protease inhibitor cocktail (complete Mini, Merck)). Proteins were quantified using the
639 Bradford method (Bio-Rad) and 30µg of total protein extract were loaded on 10% acrylamide-
640 bis-acrylamide gels or 4-20% Mini-PROTEAN TGX Precast Gels (Bio-Rad). Proteins were
641 separated by migration at 135V in 1X Tris-Glycine-SDS buffer (Euromedex). Proteins were
642 electro-transferred on a nitrocellulose membrane in 1X Tris-Glycine buffer supplemented with
643 20% ethanol. Equal loading was verified by Ponceau S staining (Merck). Membranes were
644 blocked for 1 hour at RT under stirring in 5% milk (Roth) diluted in PBS-Tween 0.2% (PBS-
645 T). Membranes were probed with the following antibodies overnight at 4°C under stirring: anti-
646 hDICER (1:1000, A301-937A, Euromedex, Bethyl), anti-PKR (1:1000, ab32506 Abcam), anti-
647 PKR (1:1000, #12297 Cell signaling), anti-p-PKR (1:1000, ab 81303 Abcam), anti-PACT
648 (1:500, ab75749 Abcam), anti-TARBP2 (1:500, sc-514124, Cliniscience, Santa Cruz), anti-
649 HA-HRP (1:10000, 12013819001 Merck, Sigma Aldrich), anti-c-Myc (1:1000, ab32072
650 Abcam), anti-p-eIF2α (1:1000, #9721 Cell signaling), anti-α-Tubulin-HRP (1:10000, 1E4C11
651 Fisher Scientific), anti-SINV capsid (1:5000, kind gift from Dr. Diane Griffin, Johns Hopkins
652 University School of Medicine, Baltimore, MD), anti-GFP (1:1000, 11814460001 Merck,
653 Sigma Aldrich), anti-GAPDH-HRP (1:10000, G9545 Merck, Sigma Aldrich), anti-SARS-CoV-
654 2 Nucleocapsid (1:1000, ab273167 Abcam), anti-AGO2 (1:250, kind gift from Pr. Gunter
655 Meister, University of Regensburg), anti-ACE2 (1:1000, AF933 Bio-Techne), anti-NF-kB/p65

656 (1:1000, #8242 Cell signaling), anti-p-NF-kB/p65 (1:1000, #3033 Cell signaling) and anti-
657 IkBα (1:1000, #4812 Cell signaling). The detection was performed using a specific secondary
658 antibody coupled to the horseradish peroxidase (HRP): anti-mouse-HRP (1:4000, A4416
659 Merck, Sigma Aldrich), anti-rabbit-HRP (1:10000, #31460 Fisher Scientific), anti-rat-HRP
660 (1:10000, #31470 Fisher Scientific) and anti-goat-HRP (1:10000, #A15999 Invitrogen).
661 Detection was done using Chemiluminescent Substrate or SuperSignal West Femto maximum
662 sensitivity substrate (Pierce, Fisher Scientific) and visualized with a Fusion FX imaging system
663 (Vilber).
664
665 **RNA extraction**
666 Total RNA was extracted using TRI Reagent solution (Invitrogen, Fisher Scientific) according
667 to the manufacturer's instructions.
668
669 **Northern blot analysis**
670 5 micrograms of total RNA were loaded on a 17.5% acrylamide-urea 4M gel and resolved in
671 1X Tris-Borate-EDTA buffer. Small RNAs were electro-transferred onto a nylon Hybond-NX
672 membrane (GE Healthcare) in 0.5X Tris-Borate-EDTA buffer. RNAs were chemically cross-
673 linked to the membrane for 90 minutes at 65°C using 1-ethyl-3-[3-
674 dimethylaminopropyl]carbodiimide hydrochloride (EDC) (Merck, Sigma Aldrich). The
675 membrane was pre-hybridized for 30 minutes in Perfect Hyb plus (Merck, Sigma Aldrich) at
676 50°C in rotation. Oligodeoxyribonucleotide probes (see Supp. Table 1) were labeled at the 5'-
677 end with 25 µCi of [γ-32P]dATP using T4 polynucleotide kinase (Fischer Scientific). The
678 unbound [γ-32P]dATP was removed with MicroSpin G-25 column (GE Healthcare) and the
679 probe was incubated overnight at 50°C with the membrane in rotation. The membrane was
680 washed twice with 5X SSC (Saline-Sodium citrate buffer, Euromedex), 0.1% SDS for 15

681 minutes at 50°C and once with 1X SSC (Euromedex), 0.1% SDS for 5 minutes at 50°C. The
682 membrane was exposed on a phosphorimaging plate in a cassette and the signal was recorded
683 using a Typhoon FLA-7000 laser scanner (GE Healthcare).
684
685 **RT-qPCR analysis**
686 DNaseI treatment was performed on 1µg of extracted RNAs (Invitrogen). DNase treated RNAs
687 were then retro-transcribed using a random nonameric primers with the SuperScript IV (SSIV)
688 reverse transcriptase according to the manufacturer's instructions (Invitrogen, Fisher
689 Scientific). Real-time quantitative PCR was performed on 1/10 dilution of cDNA using SYBR
690 green PCR master mix (Fisher Scientific) and the primers listed in Supp. Table 1.
691
692 **Strand-specific semi-quantitative RT-PCR on SINV antigenome**
693 Negative-strand-specific reverse transcription was performed using a primer specific to the 5'
694 region of the SINV plus-strand genome (nucleotides 1 to 42 – Supp. Table 1). 100 ng of RNA,
695 1µL of 2µM specific primer, 1µL of 10mM dNTPs and water up to 13µL final volume were
696 mixed and incubated at 65°C for 5 min. 4µL of 5X SSIV Buffer (Invitrogen), 1µL of 0.1M
697 DTT (dithiothreitol), 1µL of RNase inhibitor (Ribolock, Fisher Scientific) and 1µL of SSIV
698 reverse transcriptase (Invitrogen) were added and the mix was incubated at 55°C for 10 min
699 then 80°C for 10 min. 1/20 of the cDNA was amplified by PCR using the GoTaq DNA
700 polymerase mix (Promega) with specific antigenome primers (Supp. Table 1). PCR products
701 were loaded on a 1% agarose gel and gel pictures were taken with a Fusion FX imaging system
702 (Vilber).
703
704 **Immunoprecipitation**

705 Immunoprecipitations were done on tagged proteins. Cells were harvested, infected at the
706 corresponding MOI and time and washed once with ice-cold PBS (Gibco, Life Technologies)
707 and resuspended in 600µL of ice-cold lysis buffer (50mM Tris-HCl pH 7.5, 140 mM NaCl, 1.5
708 mM $MgCl_2$, 0.1% NP-40 and protease inhibitor cocktail (complete Mini, Merck, Sigma
709 Aldrich). Cells were lysed for 10 min incubation on ice and lysates were cleared with a 15 min
710 centrifugation at 12 000g and 4°C. 25µL of the lysates were kept as protein INPUT. Then,
711 samples were divided in two and 40µL of magnetic beads coated with monoclonal anti-HA or
712 anti-MYC antibodies were added (MACS purification system, Miltenyi Biotech). The samples
713 were incubated for 1 hour at 4°C under rotation. Samples were sequentially loaded onto
714 µColumns (MACS purification system, Miltenyi Biotech). The columns were washed 4 times
715 with 200µL of lysis buffer. The elution was done with 95°C-pre-heated 2X Laemmli buffer
716 (20% glycerol, 4% SDS, 125mM Tris-HCl pH 6.8, 10% (v/v) 2-β-mercaptoethanol, 0.004%
717 Bromophenol Blue). Proteins were analyzed by western blot.
718
719 **Immunostaining**
720 Cells were plated on Millicell EZ 8-well slide (Merck Millipore) and infected with the different
721 viruses at the corresponding MOI and infection time. Then, cells were fixed for 10 minutes at
722 RT with 4% formaldehyde (Merck, Sigma Aldrich) diluted in PBS 1X (Gibco). Cells were
723 incubated with a blocking solution (5% normal goat serum, 0.1% Triton X-100, PBS 1X) for
724 1h at RT. Primary J2 antibody diluted in blocking solution was added at 1:1000 dilution for 3h
725 at RT. Cells were washed three times with PBS 1X-0.1% Triton X-100 (Phosphate buffered
726 saline- Triton, PBS-T) and incubated 1h at RT in the dark with a secondary antibody solution
727 containing goat anti-mouse Alexa 594 (A11032, Invitrogen, Fisher Scientific) fluorescent-
728 coupled antibody diluted to 1:1000 in PBS-T solution. After three washes with PBS-T, cell
729 nuclei were stained with DAPI diluted to 1:5000 in PBS 1X for 2 minutes at RT in the dark

730 (Life technologies, Fischer Scientific). Slides were finally mounted on coverslips and the
731 Fluoromount-G mounting media (Southern Biotech). Images were acquired using an
732 epifluorescence BX51 (Olympus) microscope with a mercury source illuminator (U-RFL-T,
733 Olympus) and with x40 immersion oil objective.
734
735 **Small RNA cloning and sequencing**
736 NoDice FHA:DICER WT #4 or N1 #6 cells were plated in P150mm petri dishes at 25 000 000
737 cells per dish and infected the following day with SINV-GFP at an MOI of 0.02 for 24h. Cells
738 were collected in 1.3mL of ice-cold lysis buffer (50mM Tris-HCl pH 7.5, 150 mM NaCl, 5mM
739 EDTA, 1% NP-40, 0,5mM DTT, 0,1U/mL of RNase inhibitor and protease inhibitor cocktail
740 (complete Mini, Merck, Sigma Aldrich)). Cells were lysed by putting the extract on ice for
741 15min. First, human AGO proteins were immunoprecipitated from whole extract to enrich for
742 loaded small-RNAs. AGO-IP was done following the protocol described in (Hauptmann *et al*,
743 2015). Briefly, 50µL of magnetic Dynabeads coupled to G protein (Invitrogen, Fisher
744 Scientific) were coupled to anti-Flag M2 antibody (F1804, Merck, Sigma Aldrich) overnight at
745 4°C under rotation. The day after, Flag-TNRC6B WT or mutant (with Tryptophans mutated to
746 Alanines; called TNRC6B Ala) peptides were incubated with the coupled beads for 3h at 4°C
747 under rotation. Meanwhile, lysates were cleared with a centrifugation step at 10 000g for 10min
748 at 4°C and 100µL were kept as INPUT (20µL for proteins and 80µL for RNAs). Then, lysates
749 were divided in two and put on the beads coupled to the peptides and incubated at 4°C for 3h
750 under rotation. After 4 washing steps with 300µL of ice-cold washing buffer, beads were split:
751 280µL were eluted with 1mL of TRI Reagent solution (Invitrogen, Fisher Scientific) and RNAs
752 were isolated according to the manufacturer's instructions; 20µL were kept for proteins analysis
753 of IP efficiency by western blot and 20µL of 95°C-pre-heated 2X Laemmli buffer were added

754 (20% glycerol, 4% SDS, 125mM Tris-HCl pH 6.8, 10% (v/v) 2-β-mercaptoethanol, 0.004%
755 Bromophenol Blue).
756 For small RNA libraries preparation, Illumina TruSeq small RNA library preparation kit was
757 used according to the manufacturer's protocol (RS-200-0012, Illumina).
758 Samples were analyzed with a Bioanalyzer device, and only AGO-IPs with TNRC6B wild-type
759 peptide in infected conditions in triplicates were analyzed for both cell lines, while only one
760 AGO-IP TNRC6B Ala control was analyzed for each cell line.
761 Libraries were sequenced on an Illumina HiSeq 4000 sequencer as single-end 50 base reads at
762 the GenomEast platform at the Institute of Genetics and Molecular and Cellular Biology
763 (Illkirch, France). Image analysis and base calling were performed using RTA version 2.7.7
764 and bcl2fastq version 2.20.0.422.
765
766 **mRNA sequencing**
767 NoDice FHA:DICER WT #4 or N1 #6 cells were plated in P100mm petri dishes at 5 000 000
768 cells per dish and infected the following day with SINV-GFP at an MOI of 2 for 12h or 0.02
769 for 24h. Cells were collected in Trizol reagent (Invitrogen, Thermo Fisher Scientific) and RNAs
770 were isolated according to the manufacturer's instructions.
771 Library preparation and sequencing were performed at the GenomEast platform at the Institute
772 of Genetics and Molecular and Cellular Biology (Illkirch, France). RNA-Seq libraries were
773 generated according to the manufacturer's instructions from 250 ng of total RNA using the
774 Illumina Stranded mRNA Prep, Ligation kit (Reference Guide - PN 1000000124518) and IDT
775 for Illumina RNA UD Indexes Ligation (Illumina, San Diego, USA). Briefly, Oligo(dT)
776 magnetic beads were used to purify and capture the mRNA molecules containing polyA
777 tails.The purified mRNA were then fragmented at 94°C for 2 min and copied into first strand
778 complementary DNA (cDNA) using reverse transcriptase and random primers. Second strand

779 cDNA synthesis further generated blunt-ended double-stranded cDNA and incorporated dUTP
780 in place of dTTP to achieve strand specificity by quenching the second strand during
781 amplification. Following A-tailing of DNA fragments and ligation of pre-index anchors, PCR
782 amplification was used to add indexes and primer sequences and to enrich DNA libraries (30
783 sec at 98°C; [10 sec at 98°C, 30 sec at 60°C, 30 sec at 72°C] x 12 cycles; 5 min at 72°C).
784 Surplus PCR primers were further removed by purification using SPRIselect beads (Beckman-
785 Coulter, Villepinte, France) and the final libraries were checked for quality and quantified using
786 capillary electrophoresis.
787 Libraries were sequenced on an Illumina HiSeq 4000 sequencer as paired-end 100 base reads.
788 Image analysis and base calling were performed using RTA version 2.7.7 and bcl2fastq version
789 2.20.0.422.
790
791 **Bioinformatics analysis of small RNA sequencing data**
792 Sequencing reads of sRNA-seq libraries were processed and analyzed with the following
793 workflow. Cutadapt v1.16 (Martin, 2011) was first run to trim the 3' adapter (command:
794 cutadapt -a TGGAATTCTCGGGTGCCAAGG -e 0.1 --no-indels -O 6 -m 18 --discard-
795 untrimmed -o <name>-cutadapt.fastq <name>.fastq) and an additional filter was applied to only
796 keep 18- to 32-nt long trimmed reads for further analyses. Sample quality checks were
797 performed before and after these preprocessing steps using FastQC v0.11.8
798 (https://www.bioinformatics.babraham.ac.uk/projects/fastqc/). Preprocessed reads were then
799 mapped simultaneously to the human (GENCODE Human (GRCh38.p13) release 41) and
800 SINV-GFP (private sequence derived from NC_001547.1 – RefSeq database) genomes, using
801 Bowtie v1.3.1 (Langmead *et al*, 2009) (command: bowtie -q --phred33-quals -v 2 -y -a --best -
802 -strata -m 30 -x hg38coreGencodeSINVGFP <name>-preprocessed.fastq <name>-
803 hg38coreGencodeSINVGFP.bwtmap). Only alignments from the lowest mismatch stratum

804 with at most 2 mismatches were reported for each read, provided that their number was not
805 exceeding 30. For each library, small RNA reads deriving solely from SINV-GFP were
806 computationally extracted and further characterized. Representations of their length distribution
807 and localisation along the viral genome were both made in R with the ggplot2 and Bioconductor
808 Gviz (Hahne & Ivanek, 2016) packages respectively.
809
810 **Bioinformatics analysis of mRNA sequencing data**
811 RNA-seq data were processed and analyzed using the following workflow. The first 5'-end base
812 of each read, a T-overhang added during the library preparation with the Illumina Stranded
813 mRNA protocol, was first trimmed, before using Skewer v0.2.2 (Jiang *et al*, 2014) in paired-
814 end mode for average quality read filtering and adapter trimming (command: skewer -Q 25 -x
815 CTGTCTCTTATACACATCT -y CTGTCTCTTATACACATCT -l 31 -m pe -t 2 -o <name> -
816 -quiet <name>_R1.fq <name>_R2.fq). Sample quality checks were performed before and after
817 these preprocessing steps using FastQC v0.11.8
818 (https://www.bioinformatics.babraham.ac.uk/projects/fastqc/). Then, human full-length
819 protein-coding transcripts (GENCODE Human (GRCh38.p13) release 41) and SINV-GFP both
820 genomic and subgenomic transcripts (private sequence derived from NC_001547.1 – RefSeq
821 database) were quantified using Salmon v1.10.0 (Patro *et al*, 2017) in mapping-based mode
822 with the selective alignment algorithm and a decoy-aware transcriptome (command: salmon
823 quant -p 6 -i index/gencode41.hg38.sinv.decoys_index --libType A --seqBias --gcBias --
824 numBootstraps 30 -1 data/<name>_preprocessed_R1.fq.gz -2
825 data/<name>_preprocessed_R2.fq.gz -o salmon-quants/<name>). Transcript-level abundance
826 and count estimates thus obtained were next imported into R and further analyzed with the
827 tximport (Soneson *et al*, 2016) and DESeq2 (Love *et al*, 2014) packages. Briefly, original
828 transcript-level counts were summarized to gene-level estimated counts and an offset was

829 produced from transcript-level abundance estimates to correct for changes to the average
830 transcript length across samples. Differential expression analyses between tested conditions
831 were then conducted at the gene-level, and statistical significance was defined with an adjusted
832 p-value < 0.05 and an absolute log2 fold change > 1 thresholds. Finally, gene set enrichment
833 analysis (GSEA) studies were performed using the GSEA_4.3.2 Mac application, as made
834 available by the Broad Institute and the University of California, San Diego (https://www.gsea-
835 msigdb.org/gsea/index.jsp) (Mootha *et al*, 2003; Subramanian *et al*, 2005). These analyses were
836 conducted on the DESeq2 normalized counts of each comparison dataset against the Hallmark
837 Gene Sets (v2023.1) provided by the Molecular Signatures Database (MSigDB), and by using
838 the Human_Ensembl_Gene_ID_MSigDB.v2023.1.Hs.chip annotation file and all other
839 parameters by default, except the permutation type which was set to gene_set.
840 Heatmaps and volcano plots of RNA-seq differential expression data were generated in R using
841 respectively the pheatmap package and a custom Shiny application based on the ggplot2 and
842 ggrepel packages, while the global gene set enrichment dot plot was adapted from
843 VisualizeRNAseq (https://github.com/GryderArt/VisualizeRNAseq).
844
845 **Analysis of transcription factor enrichment**
846 Lists of NF-kB/p65, STAT1, STAT2, IRF2 and IRF3 regulated genes were downloaded from
847 Harmonizome (Rouillard *et al*, 2016). Genes from these lists that were differentially expressed
848 between the indicated RNAseq experimental conditions were selected, and their mRNA
849 expression log2 fold change was plotted as cumulative distribution histograms. The two-
850 sample Kolmogorov-Smirnov test was used to assess whether each distribution was statistically
851 different from the distribution of WT DICER cells infected with SINV vs. mock infected. p-
852 values are indicated on each histogram.
853

854 **Statistical analysis**

855 All the plaque assay statistical analysis was done with PRISM 9 (GraphPad) using One-way
856 ANOVA with a p-value threshold at $p<0.05$ on the logarithmic values.
857 All the qPCR statistical analysis was done with PRISM 9 (GraphPad) using One-way ANOVA
858 with a p-value threshold at $p<0.05$ on the log2 values or unpaired t-test on the log2 values.
859 Detailed statistical analysis for each figure can be found in Supplementary Table 2.
860

861 **Data availibility**

862 The sequencing data discussed in this publication have been deposited in NCBI's Gene
863 Expression Omnibus (Edgar *et al*, 2002) and are accessible through GEO Series accession
864 numbers XXX and YYY (attribution pending).
865

866 **SUPPLEMENTARY DATA**

867 Supplementary data accompany this manuscript, they consist of Supplementary Figures and
868 Tables Legends, six Supplementary Figures and two Supplementary Tables.
869

870 **FUNDING INFORMATION**

871 This work of the Interdisciplinary Thematic Institute IMCbio+, as part of the ITI 2021-2028
872 program of the University of Strasbourg, CNRS and Inserm, was supported by IdEx Unistra
873 (ANR-10-IDEX-0002), by SFRI-STRAT'US project (ANR-20-SFRI-0012), EUR IMCBio
874 (IMCBio ANR-17-EURE-0023) and Equipex Insectarium ANR-11-EQPX-0022 under the
875 framework of the French Investments for the Future Program. Sequencing was performed by
876 the GenomEast platform, a member of the 'France Génomique' consortium (ANR-10-INBS-
877 0009). MB is funded by a doctoral fellowship from the Ministère de l'enseignement supérieur,
878 de la recherche et de l'innovation and from the Fondation pour la Recherche Médicale (grant

879 number FDT202204014935). LG is funded by a postdoctoral fellowship from the Fondation
880 pour la Recherche Médicale (funding number SPF202209015746). SP also received funding
881 from the European Research Council (ERC-CoG-647455 RegulRNA).
882

883 **ACKNOWLEDGEMENTS**

884 We would like to thank members of the laboratory for fruitful discussions, as well as Pr. Petr
885 Svoboda (Institute of Molecular Genetics of the Czech Academy of Sciences, Prag) for sharing
886 unpublished data and exchanging ideas.
887

REFERENCES

Ahmad S & Hur S (2015) Helicases in Antiviral Immunity: Dual Properties as Sensors and Effectors. *Trends in Biochemical Sciences* 40: 576–585

Akhrymuk I, Frolov I & Frolova EI (2018) Sindbis Virus Infection Causes Cell Death by nsP2-Induced Transcriptional Shutoff or by nsP3-Dependent Translational Shutoff. *J Virol* 92: e01388-18

Baldaccini M & Pfeffer S (2021) Untangling the roles of RNA helicases in antiviral innate immunity. *PLOS Pathogens* 17: e1010072

Berlanga JJ, Ventoso I, Harding HP, Deng J, Ron D, Sonenberg N, Carrasco L & de Haro C (2006) Antiviral effect of the mammalian translation initiation factor 2alpha kinase GCN2 against RNA viruses. *EMBO J* 25: 1730–1740

Bogerd HP, Whisnant AW, Kennedy EM, Flores O & Cullen BR (2014) Derivation and characterization of Dicer- and microRNA-deficient human cells. *RNA* 20: 923–937

Bonnet MC, Weil R, Dam E, Hovanessian AG & Meurs EF (2000) PKR stimulates NF-kappaB irrespective of its kinase function by interacting with the IkappaB kinase complex. *Mol Cell Biol* 20: 4532–4542

Christian F, Smith EL & Carmody RJ (2016) The Regulation of NF-κB Subunits by Phosphorylation. *Cells* 5: 12

Chukwurah E & Patel RC (2018) Stress-induced TRBP phosphorylation enhances its interaction with PKR to regulate cellular survival. *Sci Rep* 8

Daher A, Laraki G, Singh M, Melendez-Peña CE, Bannwarth S, Peters AHFM, Meurs EF, Braun RE, Patel RC & Gatignol A (2009) TRBP Control of PACT-Induced Phosphorylation of Protein Kinase R Is Reversed by Stress. *Molecular and Cellular Biology* 29: 254–265

Deddouche S, Matt N, Budd A, Mueller S, Kemp C, Galiana-Arnoux D, Dostert C, Antoniewski C, Hoffmann JA & Imler J-L (2008) The DExD/H-box helicase Dicer-2 mediates the induction of antiviral activity in drosophila. *Nat Immunol* 9: 1425–1432

Dey M, Cao C, Dar AC, Tamura T, Ozato K, Sicheri F & Dever TE (2005) Mechanistic Link between PKR Dimerization, Autophosphorylation, and eIF2α Substrate Recognition. *Cell* 122: 901–913

Donnelly N, Gorman AM, Gupta S & Samali A (2013) The eIF2α kinases: their structures and functions. *Cell Mol Life Sci* 70: 3493–3511

Edgar R, Domrachev M & Lash AE (2002) Gene Expression Omnibus: NCBI gene expression and hybridization array data repository. *Nucleic Acids Res* 30: 207–210

Farabaugh KT, Krokowski D, Guan B-J, Gao Z, Gao X-H, Wu J, Jobava R, Ray G, de Jesus TJ, Bianchi MG, *et al* (2020) PACT-mediated PKR activation acts as a hyperosmotic stress intensity sensor weakening osmoadaptation and enhancing inflammation. *eLife* 9: e52241

Flemr M, Malik R, Franke V, Nejepinska J, Sedlacek R, Vlahovicek K & Svoboda P (2013) A Retrotransposon-Driven Dicer Isoform Directs Endogenous Small Interfering RNA Production in Mouse Oocytes. *Cell* 155: 807–816

Gibbings D, Mostowy S, Jay F, Schwab Y, Cossart P & Voinnet O (2012) Selective autophagy degrades DICER and AGO2 and regulates miRNA activity. *Nat Cell Biol* 14: 1314–1321

932 Gil J, Rullas J, García MA, Alcamí J & Esteban M (2001) The catalytic activity of dsRNA-
933 dependent protein kinase, PKR, is required for NF-κB activation. *Oncogene* 20: 385–394
934 Girardi E, Lefèvre M, Chane-Woon-Ming B, Paro S, Claydon B, Imler J-L, Meignin C &
935 Pfeffer S (2015) Cross-species comparative analysis of Dicer proteins during Sindbis
936 virus infection. *Sci Rep* 5: 10693
937 Guo Z, Li Y & Ding S-W (2019) Small RNA-based antimicrobial immunity. *Nat Rev Immunol*
938 19: 31–44
939 Gurung C, Fendereski M, Sapkota K, Guo J, Huang F & Guo Y-L (2021) Dicer represses the
940 interferon response and the double-stranded RNA-activated protein kinase pathway
941 in mouse embryonic stem cells. *Journal of Biological Chemistry* 296: 100264
942 Hahne F & Ivanek R (2016) Visualizing Genomic Data Using Gviz and Bioconductor. *Methods*
943 *Mol Biol* 1418: 335–351
944 Hauptmann J, Schraivogel D, Bruckmann A, Manickavel S, Jakob L, Eichner N, Pfaff J, Urban
945 M, Sprunck S, Hafner M, *et al* (2015) Biochemical isolation of Argonaute protein
946 complexes by Ago-APP. *Proc Natl Acad Sci U S A* 112: 11841–11845
947 Hoffmann M, Kleine-Weber H, Schroeder S, Krüger N, Herrler T, Erichsen S, Schiergens TS,
948 Herrler G, Wu N-H, Nitsche A, *et al* (2020) SARS-CoV-2 Cell Entry Depends on ACE2
949 and TMPRSS2 and Is Blocked by a Clinically Proven Protease Inhibitor. *Cell* 181: 271-
950 280.e8
951 Ishii T, Kwon H, Hiscott J, Mosialos G & Koromilas AE (2001) Activation of the IκBα kinase
952 (IKK) complex by double-stranded RNA-binding defective and catalytic inactive mutants
953 of the interferon-inducible protein kinase PKR. *Oncogene* 20: 1900–1912
954 Ito T, Yang M & May WS (1999) RAX, a Cellular Activator for Double-stranded RNA-
955 dependent Protein Kinase during Stress Signaling *. *Journal of Biological Chemistry* 274:
956 15427–15432
957 Ivashkiv LB & Donlin LT (2014) Regulation of type I interferon responses. *Nature Reviews*
958 *Immunology* 14: 36–49
959 Jiang D, Guo H, Xu C, Chang J, Gu B, Wang L, Block TM & Guo J-T (2008) Identification of
960 Three Interferon-Inducible Cellular Enzymes That Inhibit the Replication of Hepatitis C
961 Virus. *Journal of Virology* 82: 1665–1678
962 Jiang H, Lei R, Ding S-W & Zhu S (2014) Skewer: a fast and accurate adapter trimmer for
963 next-generation sequencing paired-end reads. *BMC Bioinformatics* 15: 182
964 Jm T, Wb K, Kd R & Hw H (2003) Sindbis virus vectors designed to express a foreign protein
965 as a cleavable component of the viral structural polyprotein. *Journal of virology* 77
966 Kanarek N & Ben-Neriah Y (2012) Regulation of NF-κB by ubiquitination and degradation of
967 the IκBs. *Immunol Rev* 246: 77–94
968 Kennedy EM, Whisnant AW, Kornepati AVR, Marshall JB, Bogerd HP & Cullen BR (2015)
969 Production of functional small interfering RNAs by an amino-terminal deletion mutant
970 of human Dicer. *Proc Natl Acad Sci USA* 112: E6945-6954
971 Kong J, Bie Y, Ji W, Xu J, Lyu B, Xiong X, Qiu Y & Zhou X (2023) Alphavirus infection
972 triggers antiviral RNAi immunity in mammals. *Cell Rep* 42: 112441
973 Langmead B, Trapnell C, Pop M & Salzberg SL (2009) Ultrafast and memory-efficient
974 alignment of short DNA sequences to the human genome. *Genome Biol* 10: R25
975 Lehman CW, Smith A, Kelly J, Jacobs JL, Dinman JD & Kehn-Hall K (2022) EGR1

976 Upregulation during Encephalitic Viral Infections Contributes to Inflammation and Cell
977 Death. *Viruses* 14: 1210
978 Love MI, Huber W & Anders S (2014) Moderated estimation of fold change and dispersion for
979 RNA-seq data with DESeq2. *Genome Biol* 15: 550
980 Ma E, MacRae IJ, Kirsch JF & Doudna JA (2008) Autoinhibition of Human Dicer by Its
981 Internal Helicase Domain. *Journal of Molecular Biology* 380: 237–243
982 Maillard PV, Ciaudo C, Marchais A, Li Y, Jay F, Ding SW & Voinnet O (2013) Antiviral RNA
983 interference in mammalian cells. *Science* 342: 235–238
984 Maillard PV, Van der Veen AG, Deddouche-Grass S, Rogers NC, Merits A & Reis e Sousa C
985 (2016) Inactivation of the type I interferon pathway reveals long double-stranded RNA-
986 mediated RNA interference in mammalian cells. *EMBO J* 35: 2505–2518
987 Manjunath L, Oh S, Ortega P, Bouin A, Bournique E, Sanchez A, Martensen PM, Auerbach
988 AA, Becker JT, Seldin M, *et al* (2023) APOBEC3B drives PKR-mediated translation
989 shutdown and protects stress granules in response to viral infection. *Nat Commun* 14: 820
990 Martin M (2011) Cutadapt removes adapter sequences from high-throughput sequencing reads.
991 *EMBnet.journal* 17: 10–12
992 Meister G & Tuschl T (2004) Mechanisms of gene silencing by double-stranded RNA. *Nature*
993 431: 343–9
994 Montavon TC, Baldaccini M, Lefèvre M, Girardi E, Chane-Woon-Ming B, Messmer M,
995 Hammann P, Chicher J & Pfeffer S (2021) Human DICER helicase domain recruits PKR
996 and modulates its antiviral activity. *PLoS Pathog* 17: e1009549
997 Mootha VK, Lindgren CM, Eriksson K-F, Subramanian A, Sihag S, Lehar J, Puigserver P,
998 Carlsson E, Ridderstråle M, Laurila E, *et al* (2003) PGC-1alpha-responsive genes
999 involved in oxidative phosphorylation are coordinately downregulated in human diabetes.
1000 *Nat Genet* 34: 267–273
1001 Mueller S, Gausson V, Vodovar N, Deddouche S, Troxler L, Perot J, Pfeffer S, Hoffmann JA,
1002 Saleh M-C & Imler J-L (2010) RNAi-mediated immunity provides strong protection
1003 against the negative-strand RNA vesicular stomatitis virus in Drosophila. *Proceedings of*
1004 *the National Academy of Sciences* 107: 19390–19395
1005 Nielsen CPS, Han L, Arribas-Hernández L, Karelina D, Petersen M & Brodersen P (2023)
1006 Sensing of viral RNA in plants via a DICER-LIKE Ribonuclease. 2023.01.10.523395
1007 doi:10.1101/2023.01.10.523395 [PREPRINT]
1008 Nilsson-Payant BE, Uhl S, Grimont A, Doane AS, Cohen P, Patel RS, Higgins CA, Acklin JA,
1009 Bram Y, Chandar V, *et al* (2021) The NF-κB Transcriptional Footprint Is Essential for
1010 SARS-CoV-2 Replication. *Journal of Virology* 95: 10.1128/jvi.01257-21
1011 Patro R, Duggal G, Love MI, Irizarry RA & Kingsford C (2017) Salmon provides fast and bias-
1012 aware quantification of transcript expression. *Nat Methods* 14: 417–419
1013 Pichlmair A & Reis e Sousa C (2007) Innate recognition of viruses. *Immunity* 27: 370–383
1014 Pierce JW, Schoenleber R, Jesmok G, Best J, Moore SA, Collins T & Gerritsen ME (1997)
1015 Novel inhibitors of cytokine-induced IkappaBalpha phosphorylation and endothelial cell
1016 adhesion molecule expression show anti-inflammatory effects in vivo. *J Biol Chem* 272:
1017 21096–21103
1018 Poirier EZ, Buck MD, Chakravarty P, Carvalho J, Frederico B, Cardoso A, Healy L, Ulferts R,
1019 Beale R & Reis e Sousa C (2021) An isoform of Dicer protects mammalian stem cells

1020 against multiple RNA viruses. *Science* 373: 231–236
1021 Raven JF, Wang S, Kazemi S, Baltzis D, Hatzoglou M, Tremblay ML & Koromilas AE (2006)
1022 The eIF2α kinase PKR is a negative regulator of Stat1 and Stat3. *The FASEB Journal* 20:
1023 A496–A496
1024 Richardson SJ, Willcox A, Hilton DA, Tauriainen S, Hyoty H, Bone AJ, Foulis AK & Morgan
1025 NG (2010) Use of antisera directed against dsRNA to detect viral infections in formalin-
1026 fixed paraffin-embedded tissue. *J Clin Virol* 49: 180–185
1027 Rouillard AD, Gundersen GW, Fernandez NF, Wang Z, Monteiro CD, McDermott MG &
1028 Ma'ayan A (2016) The harmonizome: a collection of processed datasets gathered to serve
1029 and mine knowledge about genes and proteins. *Database* 2016: baw100
1030 Ryman KD, White LJ, Johnston RE & Klimstra WB (2002) Effects of PKR/RNase L-
1031 Dependent and Alternative Antiviral Pathways on Alphavirus Replication and
1032 Pathogenesis. *Viral Immunology* 15: 53–76
1033 Soneson C, Love M & Robinson M (2016) Differential analyses for RNA-seq: transcript-level
1034 estimates improve gene-level inference. doi:10.12688/f1000research.7563.2
1035 [PREPRINT]
1036 Subramanian A, Tamayo P, Mootha VK, Mukherjee S, Ebert BL, Gillette MA, Paulovich A,
1037 Pomeroy SL, Golub TR, Lander ES, *et al* (2005) Gene set enrichment analysis: a
1038 knowledge-based approach for interpreting genome-wide expression profiles. *Proc Natl*
1039 *Acad Sci U S A* 102: 15545–15550
1040 Takahashi T, Nakano Y, Onomoto K, Murakami F, Komori C, Suzuki Y, Yoneyama M & Ui-
1041 Tei K (2018a) LGP2 virus sensor regulates gene expression network mediated by TRBP-
1042 bound microRNAs. *Nucleic Acids Res* 46: 9134–9147
1043 Takahashi T, Nakano Y, Onomoto K, Yoneyama M & Ui-Tei K (2018b) Virus Sensor RIG-I
1044 Represses RNA Interference by Interacting with TRBP through LGP2 in Mammalian
1045 Cells. *Genes (Basel)* 9
1046 Taylor DR, Tian B, Romano PR, Hinnebusch AG, Lai MMC & Mathews MB (2001) Hepatitis
1047 C Virus Envelope Protein E2 Does Not Inhibit PKR by Simple Competition with
1048 Autophosphorylation Sites in the RNA-Binding Domain. *Journal of Virology* 75: 1265–
1049 1273
1050 tenOever BR (2016) The Evolution of Antiviral Defense Systems. *Cell Host & Microbe* 19:
1051 142–149
1052 Thomas JM, Klimstra WB, Ryman KD & Heidner HW (2003) Sindbis virus vectors designed
1053 to express a foreign protein as a cleavable component of the viral structural polyprotein.
1054 *J Virol* 77: 5598–5606
1055 van der Veen AG, Maillard PV, Schmidt JM, Lee SA, Deddouche-Grass S, Borg A, Kjær S,
1056 Snijders AP & Reis e Sousa C (2018) The RIG-I-like receptor LGP2 inhibits Dicer-
1057 dependent processing of long double-stranded RNA and blocks RNA interference in
1058 mammalian cells. *EMBO J* 37
1059 Weber F, Wagner V, Rasmussen SB, Hartmann R & Paludan SR (2006) Double-Stranded RNA
1060 Is Produced by Positive-Strand RNA Viruses and DNA Viruses but Not in Detectable
1061 Amounts by Negative-Strand RNA Viruses. *J Virol* 80: 5059–5064
1062 Wilham JM, Orrú CD, Bessen RA, Atarashi R, Sano K, Race B, Meade-White KD, Taubner
1063 LM, Timmes A & Caughey B (2010) Rapid End-Point Quantitation of Prion Seeding

1064 Activity with Sensitivity Comparable to Bioassays. *PLOS Pathogens* 6: e1001217
1065 Williams BR (1999) PKR; a sentinel kinase for cellular stress. *Oncogene* 18: 6112–6120
1066 Wulff NH, Tzatzaris M & Young PJ (2012) Monte Carlo simulation of the Spearman-Kaerber
1067 TCID50. *Journal of Clinical Bioinformatics* 2: 5
1068 Yeh JX, Park E, Schultz KLW & Griffin DE (2019) NF-κB Activation Promotes Alphavirus
1069 Replication in Mature Neurons. *Journal of Virology* 93: e01071-19
1070 Zapletal D, Taborska E, Pasulka J, Malik R, Kubicek K, Zanova M, Much C, Sebesta M,
1071 Buccheri V, Horvat F, *et al* (2022) Structural and functional basis of mammalian
1072 microRNA biogenesis by Dicer. *Molecular Cell* 82: 4064-4079.e13
1073 Zhang Y, Xu Y, Dai Y, Li Z, Wang J, Ye Z, Ren Y, Wang H, Li W, Lu J, *et al* (2021) Efficient
1074 Dicer processing of virus-derived double-stranded RNAs and its modulation by RIG-I-
1075 like receptor LGP2. *PLOS Pathogens* 17: e1009790
1076

1077 **FIGURE LEGENDS**

1078 **Figure 1. Analysis of Dicer N1 effect on SINV replication**

1079 **A,** Mean (+/- SEM) of SINV, SINV-GFP and SINV-2A-GFP viral titers in NoDice
1080 FHA:DICER WT #4 and N1 #6 infected at an MOI ranging from 0.001 to 1 for 24h (n = 3)
1081 from plaque assay quantification. Ordinary two-way ANOVA test with Bonferroni correction.
1082 ***: $p < 0.001$; ****: $p < 0.0001$. **B,** Western blot analysis of DICER, p-PKR, PKR, CAPSID
1083 and GFP expression in SINV, SINV-GFP and SINV-2A-GFP infected NoDice FHA:DICER
1084 WT #4 and N1 #6 cells at an MOI of 0.02 for 24h. Gamma-Tubulin was used as loading control.
1085 **C,** Immunofluorescence analysis on NoDice FHA:DICER WT #4 and N1 #6 cells in mock,
1086 SINV, SINV-GFP and SINV-2A-GFP infected cells at an MOI of 0.02 for 24h. J2 antibody
1087 (red) was used to detect dsRNA upon infection. DAPI was used to stain the nuclei (blue).
1088 Magnification 40X; scale bar = 100 µm. **D,** RT-qPCR on SINV genome in NoDice
1089 FHA:DICER WT #4 and N1 #6 cells infected with SINV-GFP at an MOI of 0.02 for 24h. Mean
1090 (+/- SEM); n = 3. Unpaired t-test. ****: $p < 0.0001$.

1091

1092 **Figure 2. Dicer N1 activity against several viruses**

1093 **A,** (Top) Mean (+/- SEM) of SFV viral titers in NoDice FHA:DICER WT #4 and N1 #6 infected
1094 at an MOI of 1.10^{-4} for 24h (n = 3) from plaque assay quantification. Unpaired t-test. *: $p <$
1095 0.05. (Bottom) Immunofluorescence analysis on NoDice FHA:DICER WT #4 and N1 #6 cells
1096 in SFV infected cells. J2 antibody (red) was used to detect dsRNA upon infection. DAPI was
1097 used to stain the nuclei (blue). Magnification 40X; scale bar = 100 µm. **B,** (Top) Mean (+/-
1098 SEM) of EV71 viral titers in NoDice FHA:DICER WT #4 and N1 #6 infected at an MOI of 0.1
1099 for 24h (n = 3) from TCID50 quantification. Unpaired t-test. *: $p < 0.05$. (Bottom)
1100 Immunofluorescence analysis on NoDice FHA:DICER WT #4 and N1 #6 cells in EV71
1101 infected cells. J2 antibody (red) was used to detect dsRNA upon infection. DAPI was used to

1102 stain the nuclei (blue). Magnification 40X; scale bar = 100 µm. **C,** (Top) Mean (+/- SEM) of
1103 VSV-GFP viral titers in NoDice FHA:DICER WT #4 and N1 #6 infected at an MOI of 1.10^{-5}
1104 for 24h (n = 3) from plaque assay quantification. Unpaired t-test. ns: non-significant. (Bottom)
1105 Immunofluorescence analysis on NoDice FHA:DICER WT #4 and N1 #6 cells in VSV-GFP
1106 infected cells. J2 antibody (red) was used to detect dsRNA upon infection. DAPI was used to
1107 stain the nuclei (blue). Magnification 40X; scale bar = 100 µm. **D,** Western blot analysis of
1108 human ACE2 expression in NoDice FHA:DICER WT #4 and N1 #6. Gamma-Tubulin was used
1109 as a loading control. **E,** Western blot analysis of DICER, p-PKR, PKR and NUCLEOCAPSID
1110 expression in SARS-CoV-2 infected NoDice FHA:DICER WT #4 and N1 #6 cells at an MOI
1111 of 0.001 for 48h. GAPDH was used as loading control. **F,** Mean (+/- SEM) of SARS-CoV-2
1112 viral titers in NoDice FHA:DICER WT #4 and N1 #6 infected at an MOI of 0.001 for 48h (n =
1113 3) from TCID50 quantification. Unpaired t-test. *: $p < 0.05$. **G,** Immunofluorescence analysis
1114 on NoDice FHA:DICER WT #4 and N1 #6 cells in SARS-CoV-2 infected cells at an MOI of
1115 0.001 for 48h. J2 antibody (red) was used to detect dsRNA upon infection. DAPI was used to
1116 stain the nuclei (blue). Magnification 40X; scale bar = 100 µm. **H,** RT-qPCR on SARS-CoV-2
1117 genome (ORF1A and SPIKE) in NoDice FHA:DICER WT #4 and N1 #6 cells infected with
1118 SARS-CoV-2 at an MOI of 0.001 for 48h. Mean (+/- SEM); n = 3. Unpaired t-test. *: $p < 0.05$;
1119 ns: non-significant.
1120

1121 **Figure 3. Analysis of the importance of Dicer N1 catalytic activity in its antiviral**
1122 **phenotype**

1123 **A,** Representative histograms of the distribution of viral reads (in percent) per RNA length upon
1124 small RNA sequencing in NoDice FHA:DICER WT #4 (left) and N1 #6 (left) cells infected
1125 with SINV-GFP at an MOI of 0.02 for 24h. Blue: positive strand; red: negative strand. **B,**
1126 Representative graphs of the mapping of 22-nt-reads on SINV-GFP genome in NoDice

1127 FHA:DICER WT #4 (left) and N1 #6 (right) cells. On the bottom: magnification of the mapping
1128 for the first 1000nt. Blue: positive strand; red: negative strand. **C,** Schematic representation of
1129 two Dicer mutants, N1 and N1-CM (catalytic mutant). In N1-CM, the two catalytic mutations
1130 are highlighted in red. **D,** Western blot analysis of DICER, HA, AGO2, PKR and TRBP
1131 expression in the monoclonal cell lines NoDice FHA:DICER WT #4, N1 #6 and N1-CM #2.17.
1132 Gamma-Tubulin was used as a loading control. **E,** Northern blot analysis of mirR-16 expression
1133 in the same samples as in D. Expression of snRNA U6 was used as a loading control. **F,** Western
1134 blot analysis of DICER, p-PKR, PKR, p-eIF2α and CAPSID expression in SINV-GFP infected
1135 cells at an MOI of 0.02 for 24h. Gamma-Tubulin was used as loading control. **G,** Mean (+/-
1136 SEM) of SINV-GFP viral titers in the same samples as in D, infected at an MOI of 0.02 for 24h
1137 (n = 3) from plaque assay quantification. Ordinary one-way ANOVA test with Bonferroni
1138 correction. **: $p < 0.01$.
1139
1140 **Figure 4. Analysis of the importance of the helicase sub-domains for Dicer antiviral**
1141 **activity**
1142 **A,** Schematic representation of the different Dicer helicase subdomain mutants. **B,** Western blot
1143 analysis of HA (for Dicer) and CAPSID expression in SINV-GFP infected cells at an MOI of
1144 0.02 for 24h. Monoclonal NoDice FHA:DICER helicase mutant and their respective catalytic
1145 mutant cells are represented: WT #4, ΔHEL1 #15, ΔHEL1-CM #1, ΔHEL2 #9, ΔHEL2-CM
1146 #21, ΔHEL2i #27 and ΔHEL2i-CM #21. Gamma-Tubulin was used as loading control. **C,** Mean
1147 (+/- SEM) of SINV-GFP viral titers in the same samples as in B, infected at an MOI of 0.02 for
1148 24h (n = 3) from plaque assay quantification. Ordinary one-way ANOVA test with Bonferroni
1149 correction. ***: $p < 0.001$; ****: $p < 0.0001$; ns: non-significant. **D,** Western blot analysis of
1150 HA (for Dicer) and CAPSID expression in SINV-GFP infected cells at an MOI of 0.02 for 24h.
1151 Polyclonal NoDice FHA:DICER (left) and NoDiceΔPKR FHA:DICER (right) helicase mutant

1152 cells are represented. Gamma-Tubulin was used as loading control. **E,** Mean (+/- SEM) of
1153 SINV-GFP viral titers in the same samples as in D, infected at an MOI of 0.02 for 24h (n = 3)
1154 from plaque assay quantification. Ordinary one-way ANOVA test with Dunnett correction. *:
1155 $p < 0.05$; **: $p < 0.01$; ***: $p < 0.001$; ns: non-significant.
1156
1157 **Figure 5. Importance of PKR dimerization and/or catalytic activities in Dicer N1 antiviral**
1158 **activity**
1159 **A,** Schematic representation of PKR and its two point mutants: K296R and T451A. **B,** Western
1160 blot analysis of DICER, p-PKR, PKR, p-eIF2α and CAPSID expression in SINV-GFP infected
1161 NoDiceΔPKR FHA:DICER WT #2 with a MYC:EMPTY CTRL vector, MYC:PKR, MYC
1162 K296R or MYC:T451A cells at an MOI of 0.02 for 24h. Gamma-Tubulin was used as loading
1163 control. **C,** Mean (+/- SEM) of SINV-GFP viral titers in the same samples as in B, infected at
1164 an MOI of 0.02 for 24h (n = 3) from plaque assay quantification. Ordinary one-way ANOVA
1165 test with Dunnett correction. ns: non-significant. **D,** Western blot analysis of DICER, p-PKR,
1166 PKR, p-eIF2α and CAPSID expression in SINV-GFP infected NoDiceΔPKR FHA:DICER N1
1167 #6 with a MYC:EMPTY CTRL vector, MYC:PKR, MYC K296R or MYC:T451A cells at an
1168 MOI of 0.02 for 24h. Gamma-Tubulin was used as loading control. **E,** Mean (+/- SEM) of
1169 SINV-GFP viral titers in the same samples as in D, infected at an MOI of 0.02 for 24h (n = 3)
1170 from plaque assay quantification. Ordinary one-way ANOVA test with Dunnett correction. *:
1171 $p < 0.05$.
1172
1173 **Figure 6. Transcriptomic analysis of Dicer N1 and WT cells**
1174 **A,** Z-score hierarchical clustering heatmap of genes identified by RNA sequencing analysis as
1175 differentially expressed between WT vs. N1 cells, either mock or SINV-infected cells (MOI 2
1176 12 hpi or MOI 0.02 24 hpi). Gene clusters are delimited with black brackets and numbered from

1177 I to V. **B-D**, Volcano plot for differentially expressed genes (DEGs) between SINV-infected
1178 (MOI of 0.02 for 24h) and mock NoDice FHA:DICER WT #4 cells (B); SINV-infected and
1179 mock NoDice FHA:DICER N1 #6 cells (C); mock NoDice FHA:DICER WT #4 and mock
1180 NoDice FHA:DICER N1 #6 cells (D). Each gene is marked as a dot (red: upregulated ≥ 2-fold,
1181 blue: downregulated ≤ 2-fold, grey: unchanged). The horizontal line denotes an adjusted p-
1182 value of 0.05 and the vertical ones the Log2 fold change cut-off (-1 and 1). **E,** Biological states
1183 and processes associated terms enrichment performed with GSEA using the hallmark gene sets.
1184 Colors indicate NES (normalized enrichment score) that are either positive (red) or negative
1185 (blue). Dot size corresponds to -log10(FDR q-val) of enrichment.
1186
1187 **Figure 7. Analysis of the transcription factors involvement in Dicer N1 and WT cells**
1188 **transcriptomic changes**
1189 **A-B,** Histograms representing the cumulative probability of differentially expressed genes
1190 controlled by the transcription factors NF-kB/p65 (A) or STAT2 (B), plotted according to their
1191 Log2 fold change. The vertical lines stand for the Log2 fold change cut-off (-1 and 1). The two-
1192 sample Kolmogorov-Smirnov test was used to assess whether each distribution was statistically
1193 different from the distribution of NoDice FHA:DICER WT #4 cells infected with SINV vs.
1194 mock. p-values are indicated on each histogram. Red: WT SINV-002-24h vs WT MOCK; blue:
1195 N1 SINV-002-24h vs N1 MOCK; black: N1 MOCK vs WT MOCK. **C-D,** Z-score hierarchical
1196 clustering heatmap of genes identified by RNA sequencing analysis as differentially expressed
1197 between WT vs. N1 cells, either mock or SINV-infected cells (MOI 2 12 hpi or MOI 0.02 24
1198 hpi). Each heatmap represents differentially expressed genes controlled by one transcription
1199 factor: NF-kB/p65 (C) or STAT2 (D). **E,** RT-qPCR on upregulated genes in the N1 MOCK vs
1200 WT MOCK condition and controlled by either NF-kB/p65 or STAT2. Mean (+/- SEM); n = 3.
1201 Unpaired t-test. **: $p < 0.01$; ***: $p < 0.001$; ****: $p < 0.0001$.

1202 **Figure 8. NF-kB/p65 involvement in Dicer N1 antiviral phenotype**

1203 **A,** Western blot analysis of DICER, p-p65 and p65 (left) and DICER, p-PKR, p-eIF2α and
1204 CAPSID (right) expression in SINV-GFP infected NoDice FHA:DICER WT #4 and N1 #6
1205 cells at an MOI of 0.02 between 3 and 24h. Gamma-Tubulin was used as loading control. **B,**
1206 Western blot analysis of DICER, p-p65, p65 and CAPSID (top) and DICER and IkBα (bottom)
1207 expression in SINV-GFP infected NoDice FHA:DICER N1 #6 cells at an MOI of 0.02 for 24h.
1208 Before infection, cells were treated with the NF-kB/p65 inhibitor, BAY 11-7082 or the vehicle
1209 (DMSO) at the indicated concentrations for 1 h. Gamma-Tubulin was used as loading control.
1210 **C,** RT-qPCR on PTGS2 (NF-kB/p65 target) in NoDice FHA:DICER N1 #6 mock cells treated
1211 with BAY 11-7082 or the vehicle (DMSO) at the indicated concentrations for 1h. Mean (+/-
1212 SEM), n = 3. Ordinary one-way ANOVA with Sidak correction. **: $p < 0.01$; ns: non-
1213 significant. **D,** Mean (+/- SEM) of SINV-GFP viral titers in the same samples as in C, infected
1214 at an MOI of 0.02 for 24h (n = 3) from plaque assay quantification. Ordinary one-way ANOVA
1215 test with Dunnett correction. **: $p < 0.01$; ns: non-significant.

Figure 1

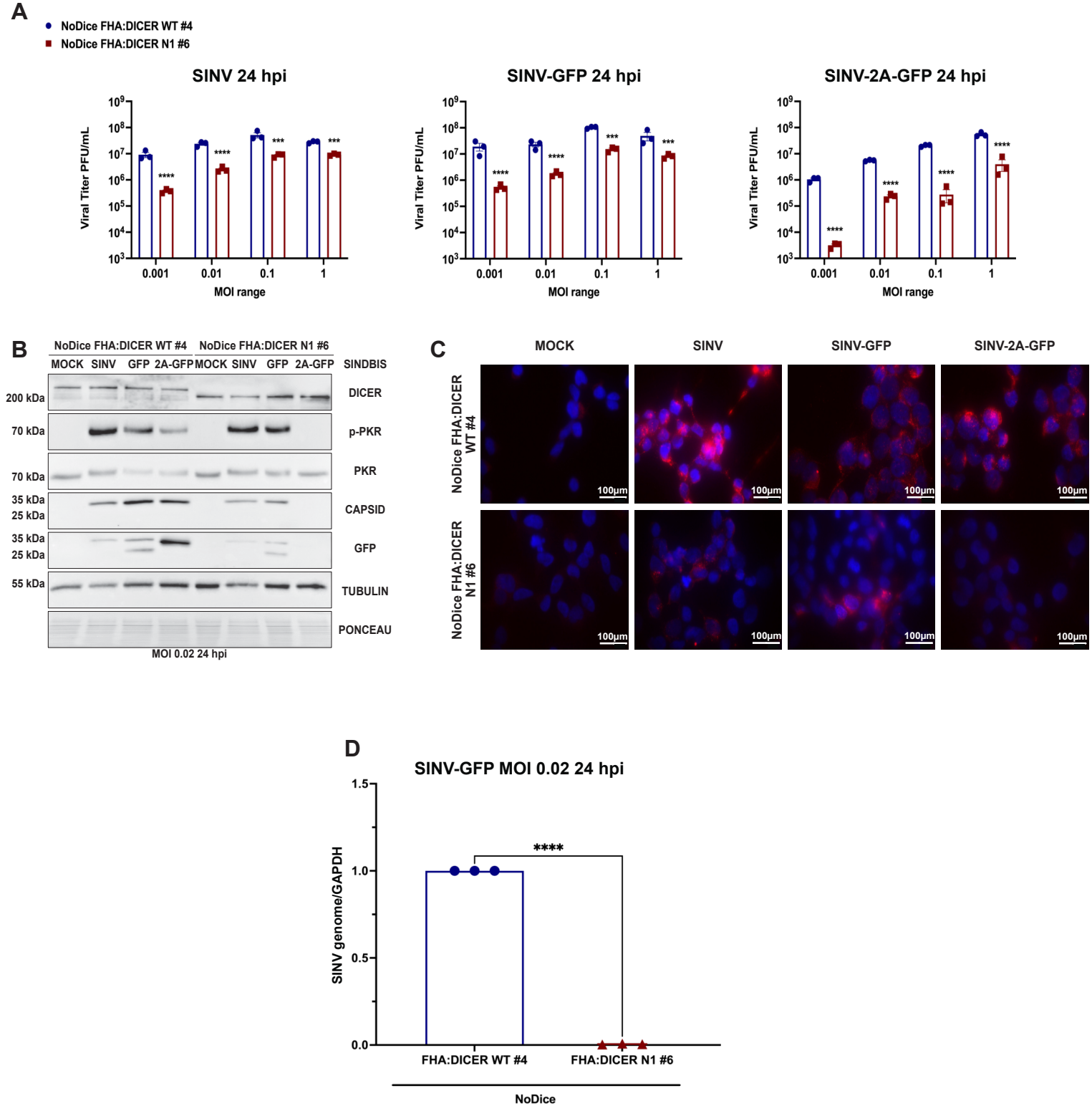
A
NoDice FHA:DICER WT #4
NoDice FHA:DICER N1 #6
SINV 24 hpi
SINV-GFP 24 hpi
SINV-2A-GFP 24 hpi
Viral Titer PFU/mL
MOI range
0.001
0.01
0.1
1
****
***
B
NoDice FHA:DICER WT #4
NoDice FHA:DICER N1 #6
MOCK SINV GFP 2A-GFP MOCK SINV GFP 2A-GFP SINDBIS
200 kDa
DICER
70 kDa
p-PKR
70 kDa
PKR
35 kDa
25 kDa
CAPSID
35 kDa
25 kDa
GFP
55 kDa
TUBULIN
PONCEAU
MOI 0.02 24 hpi
C
MOCK
SINV
SINV-GFP
SINV-2A-GFP
NoDice FHA:DICER WT #4
NoDice FHA:DICER N1 #6
100µm
D
SINV-GFP MOI 0.02 24 hpi
SINV genome/GAPDH
1.5
1.0
0.5
0.0
****
FHA:DICER WT #4
FHA:DICER N1 #6
NoDice

Figure 2

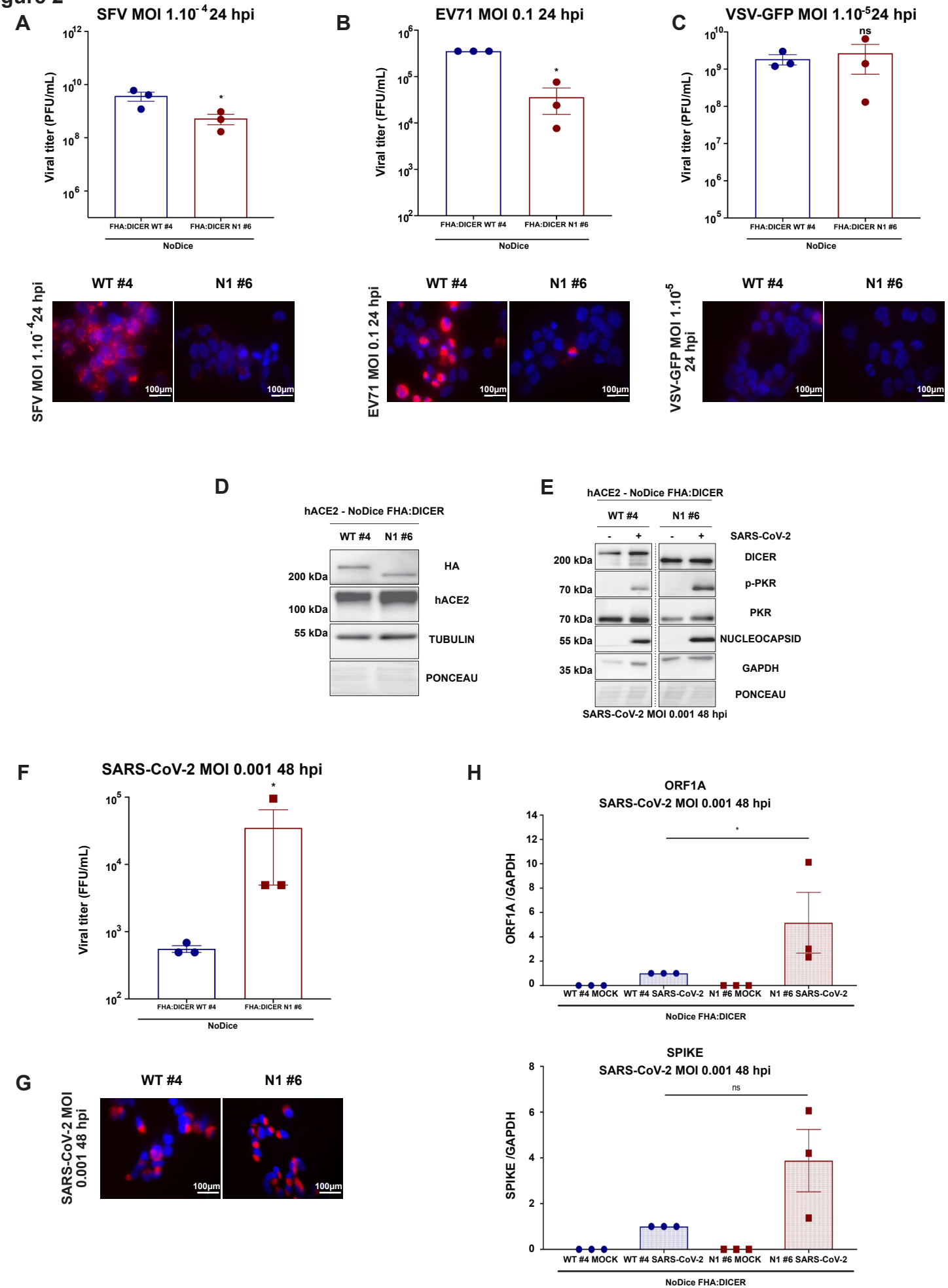
A
SFV MOI 1.10-4 24 hpi
Viral titer (PFU/mL)
FHA:DICER WT #4
FHA:DICER N1 #6
NoDice
B
EV71 MOI 0.1 24 hpi
Viral titer (FFU/mL)
C
VSV-GFP MOI 1.10-5 24 hpi
ns
WT #4
N1 #6
SFV MOI 1.10-4 24 hpi
EV71 MOI 0.1 24 hpi
VSV-GFP MOI 1.10-5 24 hpi
100µm
D
hACE2 - NoDice FHA:DICER
200 kDa
100 kDa
55 kDa
HA
hACE2
TUBULIN
PONCEAU
E
hACE2 - NoDice FHA:DICER
SARS-CoV-2
200 kDa
70 kDa
70 kDa
55 kDa
35 kDa
DICER
p-PKR
PKR
NUCLEOCAPSID
GAPDH
PONCEAU
SARS-CoV-2 MOI 0.001 48 hpi
F
SARS-CoV-2 MOI 0.001 48 hpi
Viral titer (FFU/mL)
G
SARS-CoV-2 MOI 0.001 48 hpi
H
ORF1A
SARS-CoV-2 MOI 0.001 48 hpi
ORF1A /GAPDH
WT #4 MOCK
WT #4 SARS-CoV-2
N1 #6 MOCK
N1 #6 SARS-CoV-2
NoDice FHA:DICER
SPIKE
SARS-CoV-2 MOI 0.001 48 hpi
SPIKE /GAPDH

Figure 3

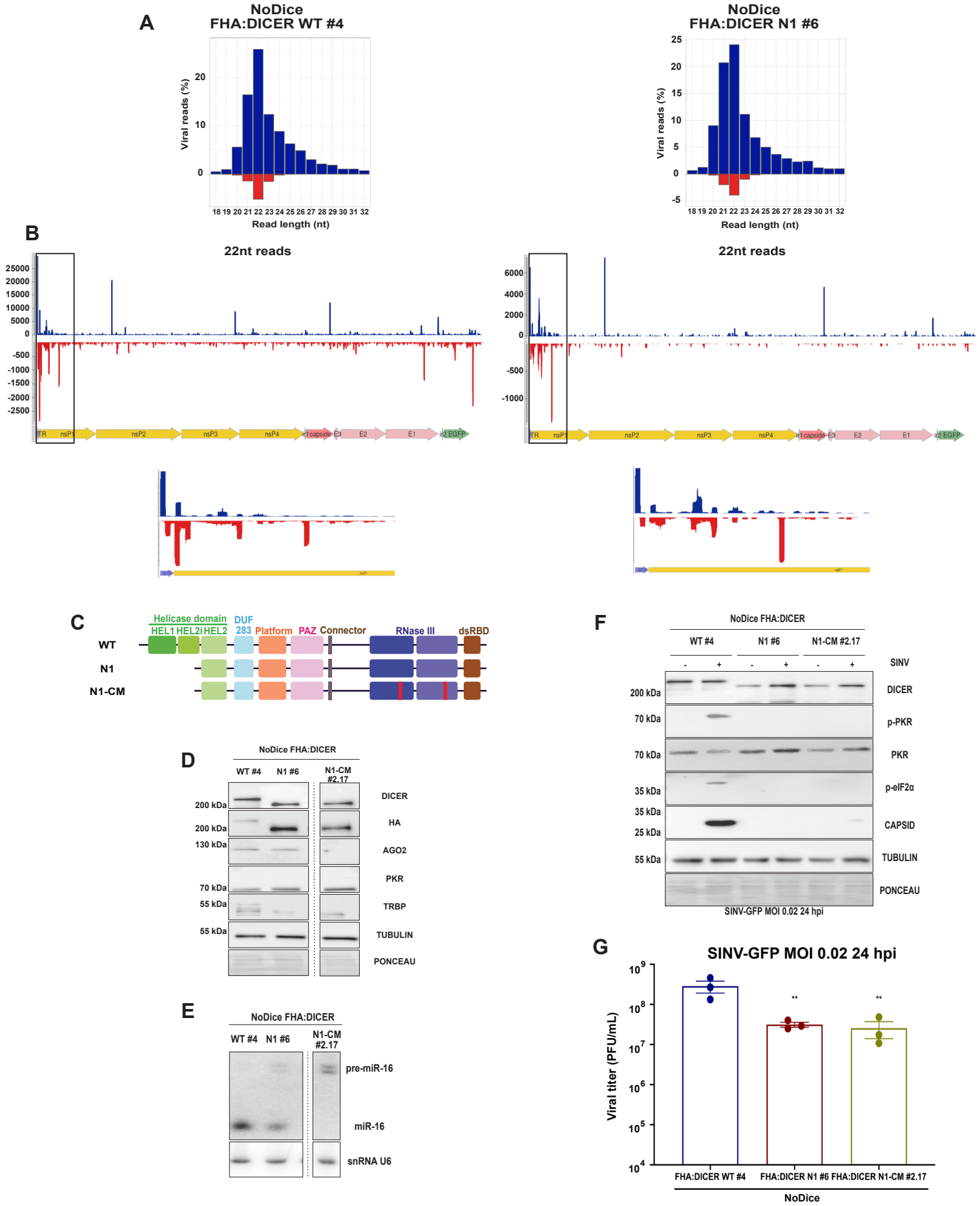
A
NoDice
FHA:DICER WT #4
Viral reads (%)
Read length (nt)
NoDice
FHA:DICER N1 #6
Viral reads (%)
Read length (nt)
B
22nt reads
22nt reads
TR
nsP1
nsP2
nsP3
nsP4
ir1 capside
E3
E2
E1
ir2 EGFP
C
Helicase domain
HEL1 HEL2i HEL2
DUF
283
Platform
PAZ
Connector
RNase III
dsRBD
WT
N1
N1-CM
D
NoDice FHA:DICER
WT #4
N1 #6
N1-CM #2.17
200 kDa
200 kDa
130 kDa
70 kDa
55 kDa
55 kDa
DICER
HA
AGO2
PKR
TRBP
TUBULIN
PONCEAU
E
NoDice FHA:DICER
WT #4
N1 #6
N1-CM #2.17
pre-miR-16
miR-16
snRNA U6
F
NoDice FHA:DICER
WT #4
N1 #6
N1-CM #2.17
SINV
200 kDa
70 kDa
70 kDa
35 kDa
35 kDa
25 kDa
55 kDa
DICER
p-PKR
PKR
p-eIF2α
CAPSID
TUBULIN
PONCEAU
SINV-GFP MOI 0.02 24 hpi
G
SINV-GFP MOI 0.02 24 hpi
Viral titer (PFU/mL)
FHA:DICER WT #4
FHA:DICER N1 #6
FHA:DICER N1-CM #2.17
NoDice

Figure 4

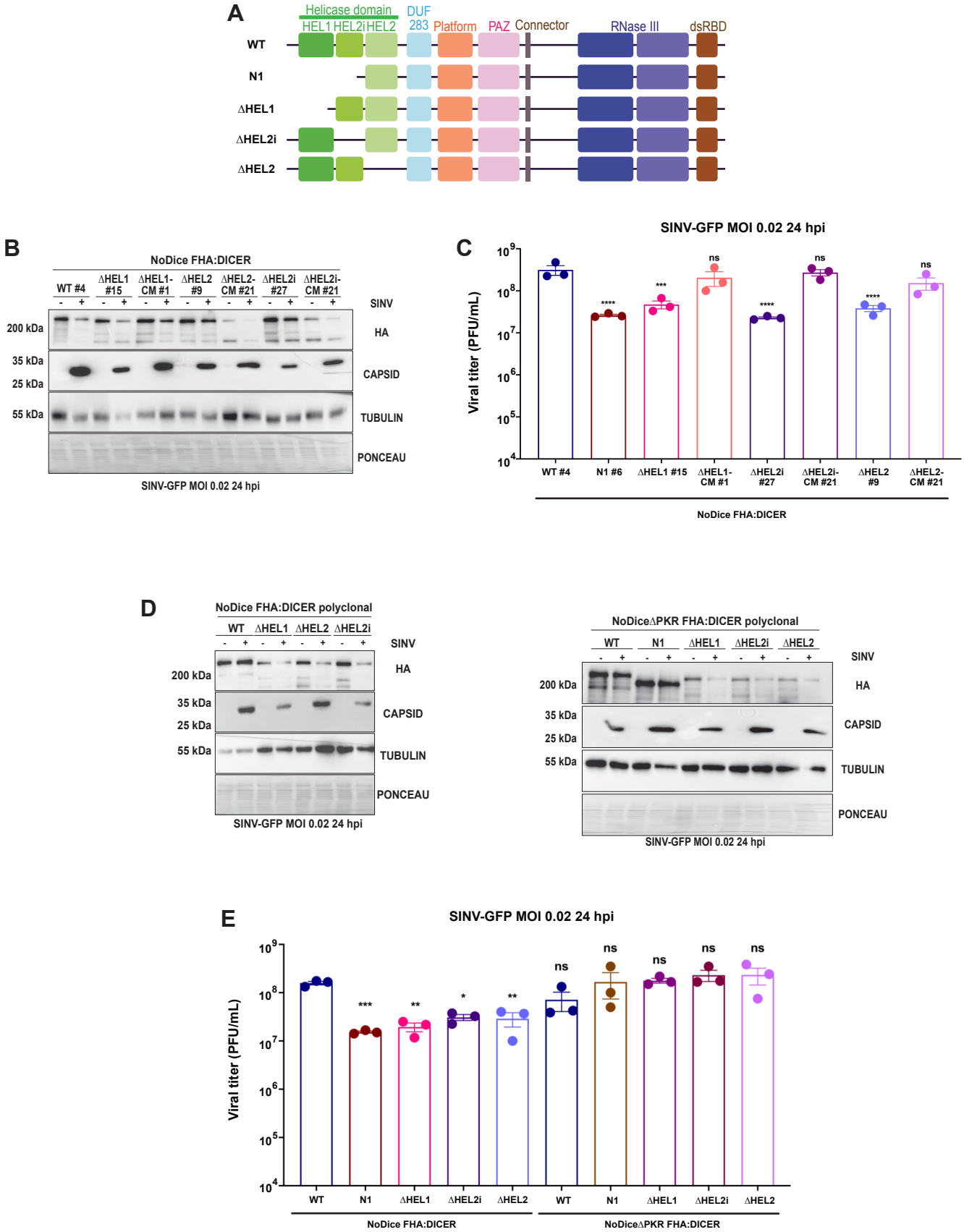
A
Helicase domain
HEL1 HEL2i HEL2
DUF 283
Platform
PAZ
Connector
RNase III
dsRBD
WT
N1
ΔHEL1
ΔHEL2i
ΔHEL2
B
NoDice FHA:DICER
WT #4
ΔHEL1 #15
ΔHEL1-CM #1
ΔHEL2 #9
ΔHEL2-CM #21
ΔHEL2i #27
ΔHEL2i-CM #21
200 kDa
35 kDa
25 kDa
55 kDa
SINV
HA
CAPSID
TUBULIN
PONCEAU
SINV-GFP MOI 0.02 24 hpi
C
SINV-GFP MOI 0.02 24 hpi
Viral titer (PFU/mL)
WT #4
N1 #6
ΔHEL1 #15
ΔHEL1-CM #1
ΔHEL2i #27
ΔHEL2i-CM #21
ΔHEL2 #9
ΔHEL2-CM #21
NoDice FHA:DICER
D
NoDice FHA:DICER polyclonal
WT
ΔHEL1
ΔHEL2
ΔHEL2i
SINV-GFP MOI 0.02 24 hpi
NoDiceΔPKR FHA:DICER polyclonal
N1
SINV-GFP MOI 0.02 24 hpi
E
SINV-GFP MOI 0.02 24 hpi
Viral titer (PFU/mL)
NoDice FHA:DICER
NoDiceΔPKR FHA:DICER

Figure 5

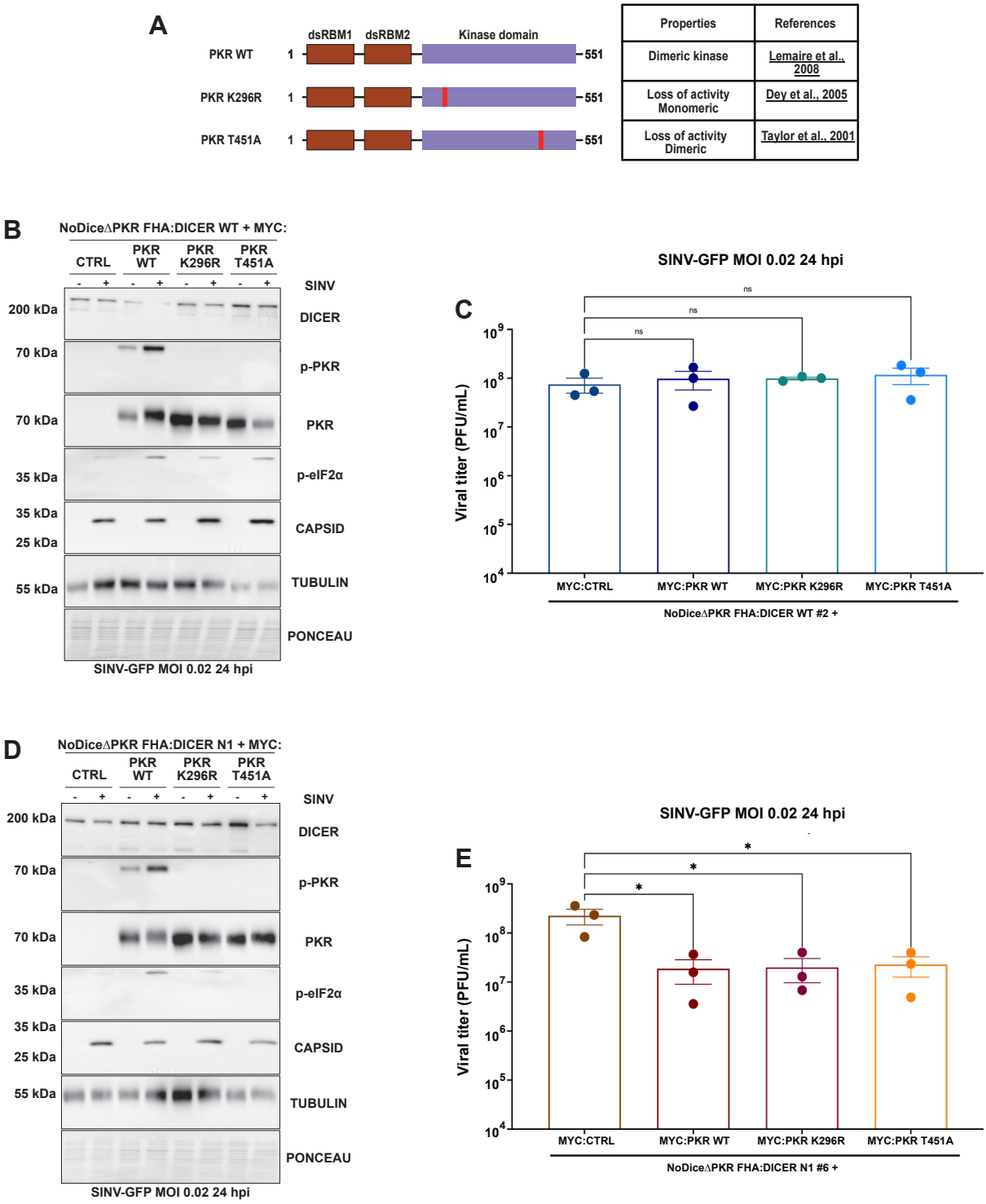
A
dsRBM1
dsRBM2
Kinase domain
PKR WT
PKR K296R
PKR T451A
1
551
Properties
References
Dimeric kinase
Lemaire et al., 2008
Loss of activity Monomeric
Dey et al., 2005
Loss of activity Dimeric
Taylor et al., 2001
B
NoDiceΔPKR FHA:DICER WT + MYC:
CTRL
PKR WT
PKR K296R
PKR T451A
SINV
200 kDa
DICER
70 kDa
p-PKR
70 kDa
PKR
35 kDa
p-eIF2α
35 kDa
25 kDa
CAPSID
55 kDa
TUBULIN
PONCEAU
SINV-GFP MOI 0.02 24 hpi
C
SINV-GFP MOI 0.02 24 hpi
Viral titer (PFU/mL)
ns
MYC:CTRL
MYC:PKR WT
MYC:PKR K296R
MYC:PKR T451A
NoDiceΔPKR FHA:DICER WT #2 +
D
NoDiceΔPKR FHA:DICER N1 + MYC:
E
SINV-GFP MOI 0.02 24 hpi
Viral titer (PFU/mL)
*
NoDiceΔPKR FHA:DICER N1 #6 +

Figure 6

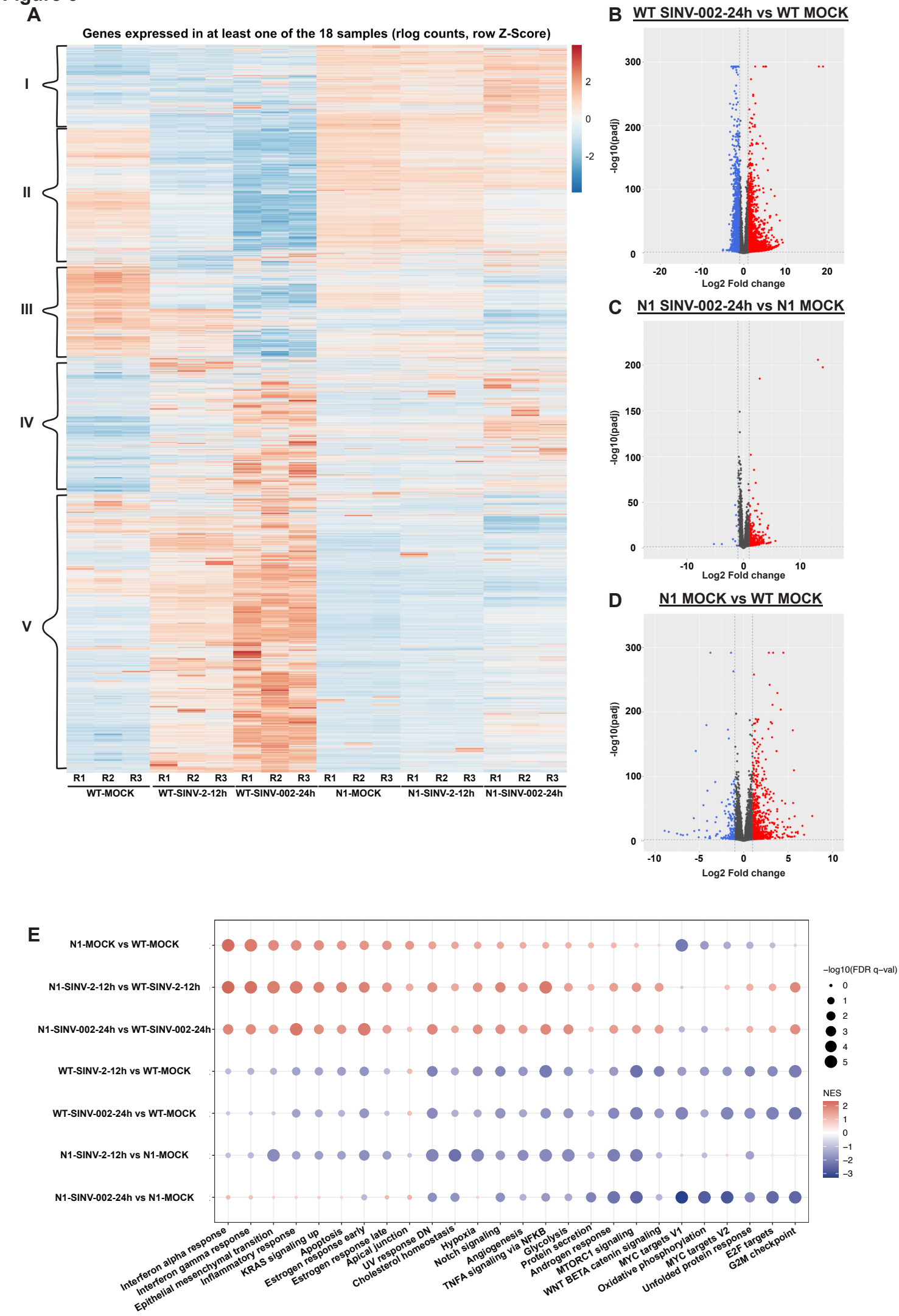
A
Genes expressed in at least one of the 18 samples (rlog counts, row Z-Score)
I
II
III
IV
V
2
0
-2
R1 R2 R3 R1 R2 R3 R1 R2 R3 R1 R2 R3 R1 R2 R3 R1 R2 R3
WT-MOCK
WT-SINV-2-12h
WT-SINV-002-24h
N1-MOCK
N1-SINV-2-12h
N1-SINV-002-24h
B
WT SINV-002-24h vs WT MOCK
-log10(padj)
Log2 Fold change
C
N1 SINV-002-24h vs N1 MOCK
-log10(padj)
Log2 Fold change
D
N1 MOCK vs WT MOCK
-log10(padj)
Log2 Fold change
E
N1-MOCK vs WT-MOCK
N1-SINV-2-12h vs WT-SINV-2-12h
N1-SINV-002-24h vs WT-SINV-002-24h
WT-SINV-2-12h vs WT-MOCK
WT-SINV-002-24h vs WT-MOCK
N1-SINV-2-12h vs N1-MOCK
N1-SINV-002-24h vs N1-MOCK
Interferon alpha response
Interferon gamma response
Epithelial mesenchymal transition
Inflammatory response
KRAS signaling up
Apoptosis
Estrogen response early
Estrogen response late
Apical junction
UV response DN
Cholesterol homeostasis
Hypoxia
Notch signaling
Angiogenesis
TNFA signaling via NFKB
Glycolysis
Protein secretion
Androgen response
MTORC1 signaling
WNT BETA catenin signaling
MYC targets V1
Oxidative phosphorylation
MYC targets V2
Unfolded protein response
E2F targets
G2M checkpoint
−log10(FDR q−val)
NES

Figure 7

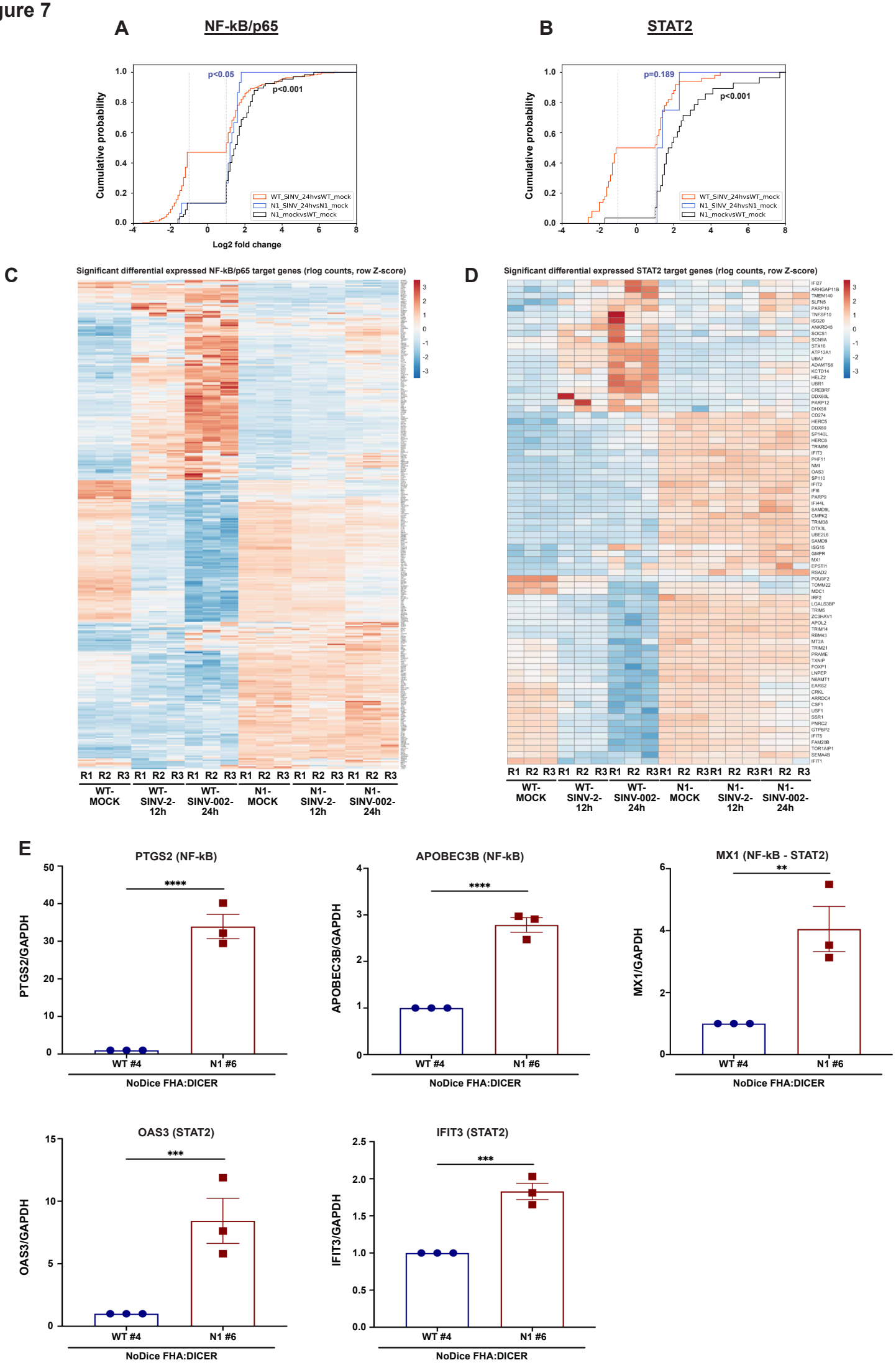
A
NF-kB/p65
p<0.05
p<0.001
Cumulative probability
Log2 fold change
WT_SINV_24hvsWT_mock
N1_SINV_24hvsN1_mock
N1_mockvsWT_mock
B
STAT2
p=0.189
p<0.001
C
Significant differential expressed NF-kB/p65 target genes (rlog counts, row Z-score)
WT-MOCK
WT-SINV-2-12h
WT-SINV-002-24h
N1-MOCK
N1-SINV-2-12h
N1-SINV-002-24h
D
Significant differential expressed STAT2 target genes (rlog counts, row Z-score)
E
PTGS2 (NF-kB)
PTGS2/GAPDH
APOBEC3B (NF-kB)
APOBEC3B/GAPDH
MX1 (NF-kB - STAT2)
MX1/GAPDH
OAS3 (STAT2)
OAS3/GAPDH
IFIT3 (STAT2)
IFIT3/GAPDH
WT #4
N1 #6
NoDice FHA:DICER

Figure 8

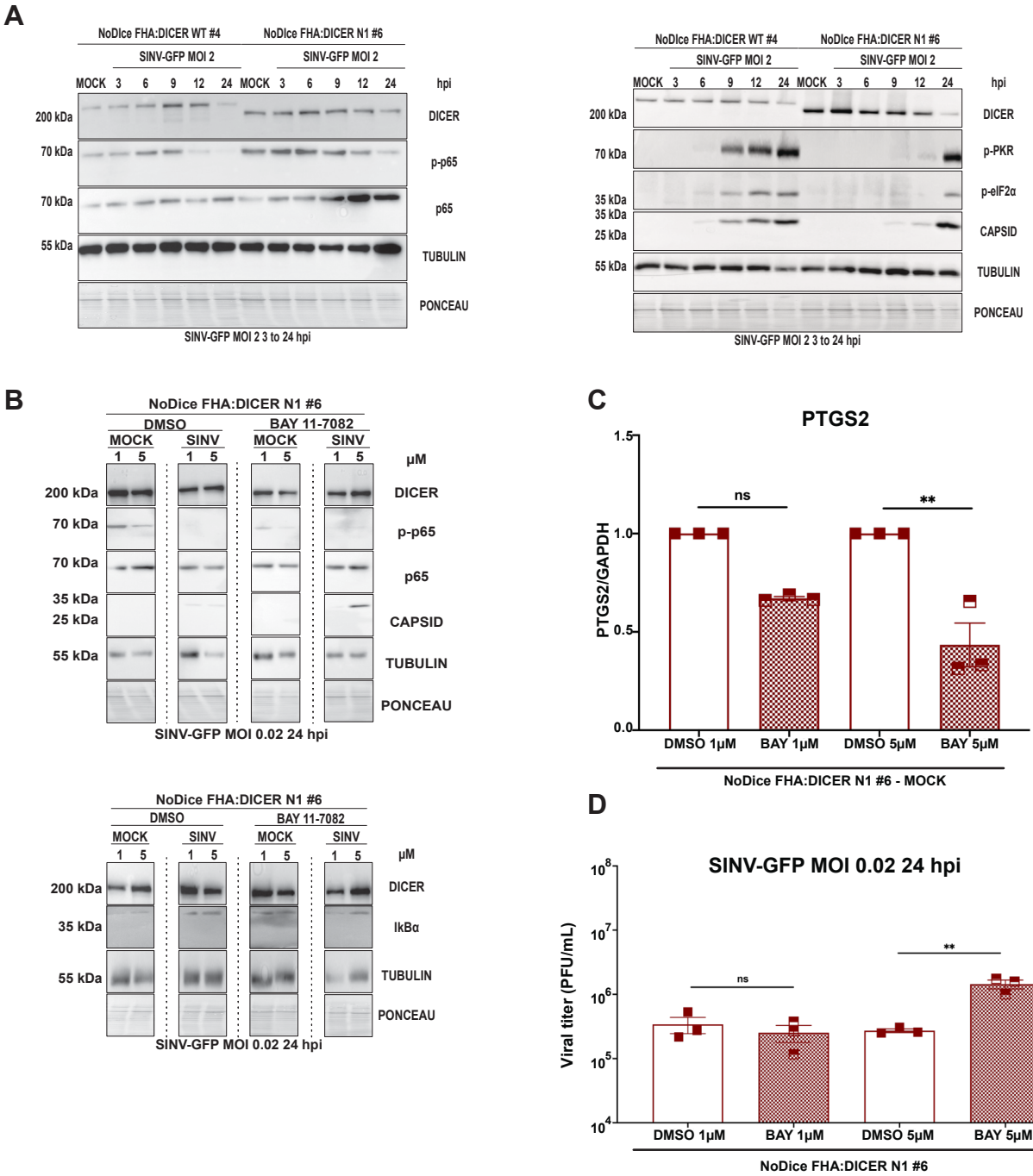
A
NoDIce FHA:DICER WT #4
NoDIce FHA:DICER N1 #6
SINV-GFP MOI 2
MOCK 3 6 9 12 24 MOCK 3 6 9 12 24
hpi
200 kDa
70 kDa
70 kDa
55 kDa
DICER
p-p65
p65
TUBULIN
PONCEAU
SINV-GFP MOI 2 3 to 24 hpi
NoDIce FHA:DICER WT #4
NoDIce FHA:DICER N1 #6
SINV-GFP MOI 2
MOCK 3 6 9 12 24 MOCK 3 6 9 12 24
hpi
200 kDa
70 kDa
35 kDa
35 kDa
25 kDa
55 kDa
DICER
p-PKR
p-eIF2α
CAPSID
TUBULIN
PONCEAU
SINV-GFP MOI 2 3 to 24 hpi
B
NoDice FHA:DICER N1 #6
DMSO
BAY 11-7082
MOCK SINV MOCK SINV
1 5 1 5 1 5 1 5
μM
200 kDa
70 kDa
70 kDa
35 kDa
25 kDa
55 kDa
DICER
p-p65
p65
CAPSID
TUBULIN
PONCEAU
SINV-GFP MOI 0.02 24 hpi
NoDice FHA:DICER N1 #6
DMSO
BAY 11-7082
MOCK SINV MOCK SINV
1 5 1 5 1 5 1 5
μM
200 kDa
35 kDa
55 kDa
DICER
IkBα
TUBULIN
PONCEAU
SINV-GFP MOI 0.02 24 hpi
C
PTGS2
PTGS2/GAPDH
1.5
1.0
0.5
0.0
ns
**
DMSO 1μM
BAY 1μM
DMSO 5μM
BAY 5μM
NoDice FHA:DICER N1 #6 - MOCK
D
SINV-GFP MOI 0.02 24 hpi
Viral titer (PFU/mL)
10^8
10^7
10^6
10^5
10^4
ns
**
DMSO 1μM
BAY 1μM
DMSO 5μM
BAY 5μM
NoDice FHA:DICER N1 #6